Carbonell, A.; López Del Rincón, C.; Daròs, J. (2019). Fast-forward Identification of Highly Effective Artificial Small RNAs Against Different Tomato spotted wilt virus Isolates. Molecular Plant-Microbe Interactions. 32(2):142-156. https://doi.org/10.1094/MPMI-05-18-0117-TA

# Fast-forward Identification of Highly Effective Artificial Small RNAs Against Different *Tomato spotted wilt virus* Isolates

Alberto Carbonell[1], Carmelo López[2] and José-Antonio Daròs[1]

*[1]Instituto de Biología Molecular y Celular de Plantas (Consejo Superior de Investigaciones Científicas-Universitat Politècnica de València), 46022 Valencia, Spain, [2]Instituto de Conservación y Mejora de la Agrodiversidad Valenciana, Universitat Politècnica de València, 46022 Valencia, Spain.*

Corresponding authors: A. Carbonell (acarbonell@ibmcp.upv.es); and J.-A. Daròs (jadaros@ibmcp.upv.es)

## ABSTRACT

**Artificial small RNAs (sRNAs), including artificial microRNAs (amiRNAs) and synthetic *trans*-acting small interfering RNAs (syn-tasiRNAs), are used to silence viral RNAs and confer antiviral resistance in plants. Here, the combined use of recent high-throughput methods for generating artificial sRNA constructs and the *Tomato spotted wilt virus* (TSWV)–*Nicotiana benthamiana* pathosystem allowed for the simple and rapid identification of amiRNAs with high anti-TSWV activity. A comparative analysis between the most effective amiRNA construct and a syn-tasiRNA construct including the four most effective amiRNA sequences showed that both were highly effective against two different TSWV isolates. These results highlight the usefulness of this high-throughput methodology for the fast-forward identification of artificial sRNAs with high antiviral activity prior to time-consuming generation of stably transformed plants.**

Artificial small RNAs (sRNAs) are 21-nucleotide (nt) RNAs designed to selectively silence transcripts, including viral RNAs, with high efficacy and specificity (Carbonell, 2017a). In plants, artificial sRNAs include artificial microRNAs (amiRNAs) used to target single or sequence related transcripts (Schwab et al., 2006), and synthetic *trans*-acting small interfering RNAs (syn-tasiRNAs) which can target multiple sites within a transcript or multiple sequence-unrelated transcripts (de la Luz Gutierrez-Nava et al., 2008; Montgomery et al., 2008a; Montgomery et al., 2008b). Both classes of artificial sRNAs exploit endogenous sRNA-directed silencing pathways for their biogenesis and function, and are synthesized *in planta* by expressing a transgene including a functional *MIRNA* or *TAS* precursor with modified miRNA or tasiRNA sequences, respectively. AmiRNAs arise from precursors with foldback structures processed by DICER-LIKE1 (DCL1), while syn-tasiRNAs are produced after processing of a *TAS* precursor by a miRNA/ARGONAUTE (AGO) complex, synthesis of dsRNA from one of the cleavage products by RNA-DEPENDENT RNA POLYMERASE 6 (RDR6), and processing of such dsRNA by DLC4 into 21-nt phased syn-tasiRNAs in register with the miRNA-guided cleavage site. Importantly, despite differing in their biogenesis pathways, both classes of artificial sRNAs associate with an AGO protein, usually AGO1, to bind and silence highly sequence complementary transcripts (Carbonell, 2017b). Methods to design, produce and validate artificial sRNA constructs have been recently optimized for high-throughput applicability and include: i) a new generation of plant “B/c” expression vectors for efficient, one-step cloning and high expression of artificial sRNAs (Carbonell et al., 2014; Carbonell et al., 2015), and ii) the P-SAMS tool (http://p-sams.carringtonlab.org) for the automated design of highly-specific plant artificial sRNAs (Fahlgren et al., 2016).

*Tomato spotted wilt virus* (TSWV) is the type species of the genus *Tospovirus*, which includes the only members of the family *Bunyaviridae* that infect plants (Plyusnin et al., 2012). TSWV, recently considered the second plant virus based on scientific and economic importance (Scholthof et al., 2011), has a wide host range that includes more than 1000 species of weeds and ornamental and

horticultural crops (Sherwood et al., 2003), and is transmitted by diverse species of thrips such as *Frankliniella occidentalis* (Whitfield et al., 2005). The genome of TSWV consists of three negative or ambisense single-stranded RNAs denoted segment large (L, 8.9 kb), segment medium (M, 4.8 kb) and segment small (S, 2.9 kb) based on their sizes (Kormlink, 2011). Segment L is completely antisense and encodes the RNA-dependent RNA polymerase (RdRp); segment M is ambisense and encodes the putative movement protein NSm and the structural proteins Gn/Gc involved in transmission by thrips; segment S is ambisense and encodes the nucleocapsid N protein and the silencing suppressor NSs (Kormlink, 2011).

Resistance to TSWV was obtained through the introgression of the two main resistance genes, *Sw5* and *Tsw*, in tomato and pepper, respectively. However, the constant emergence of resistance-breaking TSWV isolates has limited the durability of this type of resistance (Turina et al., 2016). Classic RNAi approaches such as overexpression of sense or hairpin transgenes including viral sequences (particularly from the *N* and *NSm* genes) (MacKenzie and Ellis, 1992; Prins et al., 1996; Jan et al., 2000; Sonoda and Tsumuki, 2004; Bucher et al., 2006; Peng et al., 2014), and, more recently, amiRNAs targeting the *N* gene (Mitter et al., 2016) have been also used to generate plant resistance to TSWV. Still, artificial sRNA-based strategies have not been systematically analyzed to confer highly-specific, potent and broad anti-TSWV resistance.

In this work, the goal was to explore in a simple and time-effective manner whether amiRNAs and syn-tasiRNAs could be used to protect plants against diverse TSWV isolates. For that purpose, we combined the use of recently described high-throughput methods for the design and generation of highly-specific artificial sRNA constructs (Carbonell et al., 2014; Carbonell et al., 2015; Fahlgren et al., 2016; Carbonell, 2018) and the TSWV–*Nicotiana benthamiana* pathosystem to (i) identify artificial sRNA sequences with high antiviral activity through a large functional screen of anti-TSWV amiRNAs, (ii) analyze the antiviral activity of a syn-tasiRNA construct including the most effective artificial sRNA sequences identified in the preliminary amiRNA screen; and (iii) functionally compare the anti-TSWV activity of amiRNAs and syn-tasiRNAs against two

different TSWV isolates. The main steps followed in the present work are summarized in a workflow diagram in Fig. 1, and include i) the design, selection, cloning, and functional analysis of anti-TSWV amiRNAs, ii) the generation and functional analysis of an anti-TSWV syn-tasiRNA construct including the most effective anti-TSWV amiRNA sequences, and iii) a comparative analysis of the activity of amiRNAs and syn-tasiRNAs against two different TSWV isolates.

## RESULTS

### Rational design of amiRNAs against multiple TSWV isolates

To design amiRNAs against multiple TSWV isolates, we searched the NCBI database for all complete sequences corresponding to TSWV segments L, M, and S. Twenty-nine, 65 and 61 sequences were collected, respectively. First, P-SAMS (Fahlgren et al., 2016) was used to design optimal amiRNAs against each TSWV segment with no off-targets in *Solanum lycopersicum*, TSWV natural host. No results were obtained in P-SAMS designs including either all 29, 65 or 61 sequences as input, suggesting that nucleotide variability within each segment was too high. Therefore, sequences corresponding to each segment from only six different variants isolated from *S. lycopersicum* in different regions of the world were used in subsequent P-SAMS designs (see Materials and Methods section). A list of 143, 57 and 58 optimal amiRNAs targeting specifically segments L, M and S, respectively, was obtained (Supplementary Dataset S1). Second, to identify those optimal amiRNAs targeting more conserved sites in the viral genome, the nucleotidic variability of each target site from all NCBI-collected sequences was estimated i) by calculating first the Shannon entropy value (Shannon, 1997) of each TSWV genomic position (Fig. 2A), and ii) by calculating next the entropy value of each target site as the sum of the entropy values of all target site positions. Note that the entropy values of nucleotidic positions among the three TSWV segments is highly variable as shown in Fig. 2A profiles, ranging from 0 to 1.97 (Supplementary Dataset S2). Five amiRNAs targeting segment L, five amiRNAs targeting segment M and five amiRNAs targeting segment S were selected based on the following criteria (Table 1): i) amiRNAs extensively base-pair with target

RNA (their P-SAMS score is 1 or close); ii) target sites have low variability across multiple isolates (their total entropy value is 0 or close, as shown in the entropy profiles of amiRNA target sites in Fig. 2B; and iii) target sites are distributed along the corresponding segment in RNAs of both genomic and anti-genomic polarities (Fig. 3). In particular, all amiRNAs against segment L target RdRp messenger RNA (mRNA); three and two amiRNAs against segment M target NSm viral RNA (vRNA) and mRNA, respectively; and one and four amiRNAs against segment S target N mRNA and Nss vRNA, respectively. Importantly, none of the selected amiRNAs had significant off-targets in *N. benthamiana,* the experimental host chosen for the anti-TSWV amiRNA screening, based on *TargetFinder* (Fahlgren and Carrington, 2010) computational prediction (Supplementary Table S2). Selected amiRNA sequences (Fig. 4A, 5A and 6A, Table 1, Supplementary Text S3 and Supplementary Dataset S3) were directly inserted into the *pMDC32B-AtMIR390a-B/c* expression vector optimized for one-step cloning and high expression of amiRNAs in eudicots (Carbonell et al., 2014).

**Functional analysis of anti-TSWV amiRNAs**

To begin, an extract from the well-characterized TSWV-PVR isolate (Debreczeni et al., 2015) was previously titrated to determine the minimal amount of extract that elicited symptoms in all the plants mechanically inoculated. A dilution assay showed that only the undiluted extract, obtained at a 1:20 tissue: buffer ratio, induced symptoms in upper non-inoculated tissues in 100% of the inoculated plants, between 6 and 8 days post-inoculation (dpi) (Supplementary Fig. S1). Therefore, the undiluted extract was used as TSWV-PVR inoculum.

Next, the accumulation *in planta* of each amiRNA species was analysed. Each amiRNA construct was independently agroinfiltrated in three different *N. benthamiana* plants, and infiltrated leaves were collected two days after agroinfiltration (dpa). Northern blot analysis of RNA preparations from agroinfiltrated leaves showed that amiRNAs accumulated to different levels (Supplementary Fig. S2). To functionally analyse selected amiRNAs, six *N. benthamiana* plants were agroinfiltrated independently with each of the anti-TSWV

amiRNA constructs, and then mechanically inoculated two days later with the TSWV-PVR extract. As negative controls, a set of plants was agroinfiltrated exclusively with the *35S:GUS* construct, and two other sets were agroinfiltrated independently with two anti-GUS control amiRNAs (Carbonell and Daros, 2017) and subsequently inoculated with TSWV-PVR. To determine the antiviral activity of amiRNAs, the appearance of typical TSWV-induced symptoms in inoculated tissues (local lesions) and in distant non-inoculated tissues (leaf epinasty and chlorosis) was monitored. In inoculated tissues, the number of necrotic lesions was recorded. In upper non-inoculated tissues, TSWV accumulation was analysed by ELISA at two time points (10 and 20 dpi).

Leaves agroinfiltrated with amiR-TSWV-L-3 and amiR-TSWV-L-5 targeting TSWV L segment showed very few or no lesions, respectively, when compared with leaves expressing the amiR-GUS control constructs. The rest of anti-TSWV-L amiRNAs showed a similar number of necrotic lesions compared to controls (Fig. 4). Interestingly, at 10 dpi all plants expressing amiR-TSWV-L-3 or amiR-TSWV-L-5 neither showed symptoms of infection (Fig. 4D, E) nor accumulated TSWV (Fig. 4F) in upper non-inoculated leaves. In contrast, all plants expressing amiR-TSWV-L-1, amiR-TSWV-L-2 or amiR-TSWV-L-4 displayed symptoms, although several of them with a slight delay compared to controls (Fig. 4D, E), and accumulated high levels of TSWV (Fig. 4F). At the end of the experiment (20 dpi), all plants were positive by ELISA except plants expressing amiR-TSWV-L-5 and half of the plants expressing amiR-TSWV-L-3, which did not show symptoms (Fig. 4E, Table 2). The other half of plants expressing amiR-TSWV-L-3 showed symptoms at 13 dpi, almost a week later than control plants (Fig. 4E).

In the case of amiRNAs targeting the M fragment (Fig. 5A), leaves expressing amiR-TSWV-M-3 and amiR-TSWV-M-1 showed very few or no lesions, respectively, while leaves expressing the rest of anti-TSWV-M amiRNAs displayed similar number of lesions than amiR-GUS controls (Fig. 5B, C). Importantly, the analysis of upper non-inoculated tissue at 10 dpi revealed that none of the plants expressing amiR-TSWV-M-1 and one third of the plants expressing amiR-TSWV-M-3 neither showed viral symptoms (Fig. 5D, E) nor accumulated TSWV (Fig. 5F).

In contrast, all plants expressing amiR-TSWV-M-2, amiR-TSWV-M-4 or amiR-TSWV-M-5 were symptomatic. In some of them, symptoms appeared with a slight delay compared to controls (Fig. 5D, E), and accumulated high levels of TSWV (Fig. 5F). At 20 dpi, five out of six plants expressing amiR-TSWV-M-1 and half of the plants expressing amiR-TSWV-M-3 were still symptomless and did not accumulate TSWV (Fig. 5E, F; Table 2).

Finally, all leaves expressing anti-TSWV-S amiRNAs (Fig. 6A) showed a similar number of necrotic lesions compared to controls (Fig. 6B, C). Accordingly, all plants expressing anti-TSWV-S amiRNAs showed symptoms and accumulated TSWV similarly to controls both at 10 and 20 dpi (Fig. 6D, E, F). Taken together, these results indicate that only a subset of amiRNAs targeting TSWV segments L or M were very active and blocked TSWV systemic infection in *N. benthamiana*, while none of the amiRNAs against fragment S were effective.

**Functional analysis of anti-TSWV syn-tasiRNAs**

Next, we tested if a syn-tasiRNA build on the basis of the previously selected amiRNAs could be effective against TSWV-PVR. To that purpose, the *35S:syn-tasiR-TSWV* construct was generated by introducing four syn-tasiRNA sequences corresponding to the four most effective anti-TSWV amiRNA sequences in the *pMDC32B-AtTAS1c-B/c* vector (Fig. 7A) (Carbonell et al., 2014). Similarly, the *35S:syn-tasiR-GUS* control construct was generated by introducing four syn-tasiRNA sequences corresponding to amiR-GUS-1 and amiR-GUS-2 in *pMDC32B-AtTAS1c-B/c* (Fig. 7A). The accumulation of syn-tasiRNAs derived from *35S:syn-tasiR-TSWV* and *35S:syn-tasiR-GUS* constructs was analysed in *N. benthamiana* leaves. For that purpose, each syn-tasiRNA construct was co-agroinfiltrated independently with the *35S:MIR173a* construct that expresses miR173a, which is required for *TAS1c*-dependent tasiRNA biogenesis (Montgomery et al., 2008b). Northern blot analysis of RNA preparations obtained 2 dpa from agroinfiltrated leaves confirmed syn-tasiRNA accumulation from both constructs (Supplementary Fig. S4).

As for amiRNAs, the antiviral activity of both syn-tasiRNA constructs was analysed in six *N. benthamiana* plants by co-agroinfiltrating first each syn-tasiRNA construct with *35S:MIR173a*, and inoculating then TSWV-PVR in the agroinfiltrated leaves 2 days later. As an additional control, *35S:syn-tasiR-TSWV* was co-agroinfiltrated with *35S:GUS* in the absence of *35SMIR173a*. Symptom appearance and ELISA detection of TSWV were surveyed as in the previous amiRNA assays.

Leaves co-expressing the *35S:syn-tasiR-TSWV* and *35S:MIR173a* constructs did not show necrotic lesions at 5 dpi. In contrast, all leaves co-expressing *35S:syn-tasiR-GUS* and *35S:MIR173a* or *35S:syn-tasiR-TSWV* and *35S:GUS* showed a high number of local lesions (Fig. 7B, C). At both 10 and 20 dpi, none of the plants co-expressing syn-tasiR-TSWV and miR173 showed symptoms or accumulated TSWV, in contrast with the rest of TSWV-inoculated controls (Fig. 7D-F). Altogether these results indicate that TSWV-specific syn-tasiRNAs are highly active blocking TSWV infection in *N. benthamiana*, and that their activity depends on the co-expression of miR173.

**Comparative analysis of anti-TSWV activity of amiRNAs and syn-tasiRNAs against two different TSWV isolates**

Next, we compared the inhibitory effect of amiRNAs and syn-tasiRNAs against two different TSWV isolates, PVR and LL-N.05. To simplify the analysis, we studied the antiviral effects of *35S:amiR-TSWV-L-5*, the most effective anti-TSWV amiRNA construct, and *35S:syn-tasiR-TSWV* compared with *35S:GUS*, when inoculated with the corresponding TSWV isolate. As *35S:MIR173a* had to be co-expressed with *35S:syn-tasiR-TSWV* to trigger syn-tasiRNA production, it was also co-agroinfiltrated in samples including *35S:amiR-TSWV-L-5* or *35S:GUS* for comparative purposes. Each isolate was inoculated in an independent experiment including 12 plants per block. The antiviral activity of both classes of artificial sRNAs was analysed as described in the initial amiRNA experiments.

Leaves agroinfiltrated with either *35S:amiR-TSWV-L-5* or *35S:syn-tasiR-TSWV* and subsequently inoculated with the TSWV-PVR isolate showed no or few

necrotic lesions in contrast to leaves co-expressing *35S:GUS* (Fig. 8A, B). Analysis of upper non-inoculated tissue at 10 dpi showed that none of the plants co-expressing amiR-TSWV-L-5 displayed symptoms, although in two of them TSWV was detected by ELISA (Fig. 8C-E). Similarly, only one plant co-expressing syn-tasiR-TSWV showed symptoms, while two of them accumulated TSWV-PVR (Fig. 8C-E). In contrast, all plants co-expressing *35S:GUS* showed symptoms and accumulated TSWV-PVR (Fig. 8C-E). At 20 dpi, two out of 12 plants co-expressing *35S:amiR-TSWV-L-5* or *35S:syn-tasiR-TSWV* showed symptoms (Fig. 8D) .

As described before for TSWV-PVR inoculum, an extract of *N. benthamiana* plants infected with TSWV-LL-N.05 was titrated. The dilution assay showed that both the undiluted (ratio 1:20 tissue:buffer) and the 1/10 diluted extracts induced symptoms in all inoculated plants, although these appeared earlier and more homogenously in the case of the undiluted extract (between 6 and 7 dpi, Supplementary Fig. S2). Therefore, the undiluted extract was used as TSWV-LL-N.05 inoculum. Leaves agroinfiltrated with either *35S:amiR-TSWV-L-5* or *35S:syn-tasiR-TSWV* and further inoculated with TSWV-LL-N.05 isolate showed no or few necrotic lesions in contrast with leaves expressing *35S:GUS* (Fig. 9A, B). At 10 dpi, none of the plants expressing artificial sRNAs showed symptoms (Fig. 9D), although TSWV-LL-N.05 was detected by ELISA in two of the plants expressing amiR-TSWV-L-5 and in one plant expressing syn-tasiR-TSWV (Fig. 9E). At 20 dpi, five out of 12 and three out of 12 plants expressing amiR-TSWV-L-5 and syn-tasiR-TSWV (Fig. 9D), respectively, showed symptoms and accumulated TSWV-LL-N.05 (Table 1). All combined, these results indicate that both classes of artificial sRNAs are similarly effective against two different TSWV isolates.

## DISCUSSION

### Classic RNAi approaches versus artificial sRNAs

Classic RNA interference (RNAi) strategies expressing small interfering RNAs (siRNAs) from transgene derived double-stranded RNAs (dsRNAs) of viral sequence have been widely used to confer antiviral resistance in plants (Watson et al., 2005; Pooggin, 2017). However, these strategies lack high specificity due to

the high risk of off-target effects because of the potential accidental targeting of cellular transcripts sharing high sequence complementarity with transgene-derived siRNAs. Moreover, the possibility of recombination between the transgene or transgene-derived transcripts and the genome of related pathogens cannot be discarded. These important limitations were overcome by the development of more recent, potent, and highly precise RNAi technologies based on artificial small RNAs (sRNAs) (Carbonell, 2017a).

Artificial sRNAs offer a more specific, biosafe, and versatile alternative to classic RNAi approaches for inducing antiviral resistance in plants. First, the shortness of the artificial sRNAs (21 nt) compared to longer RNAi dsRNAs (from 0.3 to several kb) facilitates the specificity analysis during the artificial sRNA design in Web-based tools such as WDM3 (Ossowski et al., 2008; Schwab et al., 2010) or P-SAMS (Fahlgren et al., 2016). The specificity analysis requires computational resources and the annotated transcriptome of the species of interest to scrutinize all possible base-pairing interactions between the candidate artificial sRNA and the complete set of host transcripts. Second, the small size of artificial sRNAs increases the biosafety of the transformed crops as it reduces the possibility of recombination with non-target viruses (Mitter et al., 2016). And third, amiRNA-mediated resistance has been proved to be more stable than siRNA-based resistance at lower temperatures (15ºC) (Niu et al., 2006). Thus, the amiRNA-mediated approach should have a broader applicability for engineering antiviral resistance in crop plants. Whether syn-tasiRNA-mediated resistance is also stable at this lower temperature needs to be proved.

**A fast-forward methodology for the identification of highly active artificial sRNA sequences**

The efficacy of a given artificial sRNA depends on multiple factors such as the degree of base-pairing between the artificial sRNA and the target RNA, or the accessibility of the target site among others. It is known that artificial sRNA efficacy positively correlates with the degree of base-pairing between the sRNA and the target RNA (Liu et al., 2014). Accordingly, automated tools for artificial sRNA

design such as WMD3 (Ossowski et al., 2008) or P-SAMS (Fahlgren et al., 2016) typically optimize for efficacy by designing sRNAs with high sequence complementarity with the target RNA. Other factors influencing artificial sRNA efficacy such as target site accessibility are much more difficult to predict and, therefore, are not taken into account during the design process (Ossowski et al., 2008; Fahlgren et al., 2016). The difficulty to predict if a particular artificial sRNA will be highly active *in vivo* makes crucial to conduct a preliminary functional screen of multiple artificial sRNAs to identify those with the highest activity before starting stable plant transformation. Pertinent to this context, it has been shown that highly active amiRNAs transiently expressed in *N. benthamiana* remain highly effective when expressed in *A. thaliana* transgenic plants (Yu and Pilot, 2014), thus further supporting the usefulness of preliminary functional screens.

Here we coupled the recently described high-throughput methods for generating artificial sRNA constructs for plants to a screening system based on agroinfiltration in *N. benthamiana* to identify optimal artificial sRNAs against an important viral pathogen of solanaceous plants, such as TSWV. Importantly, the whole process including the rational design using the P-SAMS tool (Fahlgren et al., 2016), the high-throughput generation of plant artificial sRNA constructs using the new generation of *Bsa*I/*ccd*B (B/c) vectors optimized for one-step cloning and high expression of artificial sRNA sequences (Carbonell et al., 2014; Carbonell et al., 2015), and plant agroinfiltration is completed in just a week (Carbonell, 2018). Moreover, this methodology should be of broad interest as it can be applied to search for resistance to any of the large list of viruses that infect *N. benthamiana* (Goodin et al., 2008).

**Different efficacies of anti-TSWV amiRNAs**

The amiRNA functional screen showed that only a subset of the amiRNAs tested were highly active against TSWV. In particular, only two out of five amiRNAs targeting the L segment and two out of five amiRNAs targeting the M segment were active, while none of the five amiRNAs targeting segment S were functional. Why only a subset of amiRNAs were active and others not? First, it could be

argued that more active amiRNAs may accumulate to higher levels. In our study, more active amiRNAs (amiR-TSWV-L-3, amiR-TSWV-L-5, amiR-TSWV-M1 and amiR-TSWV-M3) are among the more highly accumulated amiRNA species analyzed at 2 dpa. However, other highly accumulated amiRNAs such as amiR-TSWV-M-4 and especially amiR-TSWV-S-1 are inactive, suggesting that a high accumulation is probably required but not sufficient for an amiRNA to be active. It is also possible that different amiRNAs have different degradation rates over time, with amiRNA instability negatively affecting amiRNA activity. Second, regarding the degree of base-pairing between amiRNAs and target sites in TSWV-PVR RNAs, in our work all productive and unproductive amiRNA/target RNA interactions present only one or two missmatches within specific amiRNA regions (position 1 or 14-21) known to have a modest effect on sRNA efficacy based on studies on Arabidopsis *thaliana* miRNAs (Fahlgren and Carrington, 2010). Therefore, the degree of base-pairing between amiRNA and target RNA does not explain by itself the differences in efficacy observed between amiRNAs in our study. Moreover, the hybrid formed by the most active amiRNA (amiRNA-TSWV-L-5) and its target RNA in TSWV-PVR presents two mismatches: one at position 21 that should have a modest effect, and another at position 8 (Fig. 4A), which is included in a specific sRNA region (positions 2-14) where missmatches are known to drastically decrease sRNA activity (Fahlgren and Carrington, 2010). This result suggests that other unconventional but productive miRNA/target interactions may occur, as the one formed by an mRNA encoding the blue copper-binding protein (BCBP) and miR398 in *A. thaliana*, which includes a bulge of six nucleotides opposite to the 5' region of the miRNA (Brousse et al., 2014). And third, it is possible that other factors more difficult to predict such as target site accessibility affect more significantly the efficacy of each amiRNA as previously proposed (Carbonell and Daros, 2017). Indeed, it seems that accessibility in natural plant miRNA target sites is influenced by the local mRNA secondary structure and by the putative positioning of various mRNA binding proteins (Liu et al., 2014). For all these reasons, it is not simple to explain why a specific amiRNA is functional and another is not, as highlighted in a previous work describing that only two amiRNAs

targeting TSWV *N* gene were active, while other two amiRNAs targeting TSWV *NSs* gene were not (Mitter et al., 2016). Again, these considerations strongly support the need of a preliminary screening of multiple artificial sRNA sequences to identify those with high activity.

**amiRNA versus syn-tasiRNA**

Since their first use to confer antiviral resistance (Niu et al., 2006), amiRNAs have been widely employed to protect plants from viruses with high specificity mainly in transgenic plants [reviewed recently in (Liu et al., 2017)]. Because antiviral amiRNAs only target a single site in viral RNAs, the amiRNA-induced resistance is typically overcome because of mutations in the amiRNA target-site in the viral progeny (Lin et al., 2009; Lafforgue et al., 2011). To increase the durability of the amiRNA protection, multiple amiRNAs have been expressed from constructs including several precursors in tandem or a single polycistronic precursor (Fahim et al., 2012; Kung et al., 2012; Lafforgue et al., 2013; Kis et al., 2016). Syn-tasiRNAs have more recently emerged as an alternative to amiRNA to induce specific, potent antiviral resistance in plants. The main advantage of the syn-tasiRNA approach is that multiple artificial sRNAs can be multiplexed in a single construct, thus allowing for the simultaneous targeting of multiple target sites within a viral RNA or of multiple sequence-unrelated viruses. This should increase the durability of the syn-tasiRNA-mediated resistance as the possibility that the virus mutates all target sites to break the resistance appears unlikely (Carbonell et al., 2016). Syn-tasiRNAs have been recently shown to confer resistance against two different viruses (Chen et al., 2016) and also against viroids (Carbonell and Daros, 2017), although the durability of the protection was not analyzed. Here, the comparative analysis between the most efficient amiRNA (amiR-TSWV-L-5) and the syn-tasiRNAs showed that both classes of artificial sRNAs were highly effective against two different TSWV isolates in *N. benthamiana*.

**Conclusion**

This work describes the successful application of a fast-forward methodology for the identification of highly effective artificial sRNA sequences to suppress TSWV, an important viral pathogen causing dramatic crop losses worldwide. Our results show that both amiRNAs and syn-tasiRNAs, transiently-expressed in *N. benthamiana*, are highly effective against two different TSWV isolates. Future work is though necessary to confirm that both classes of artificial sRNAs can induce high levels of durable anti-TSWV resistance when stably expressed in transformed tomato plants. In any case, the efficient methodology described here should be of broad interest as it could be applied for the quick identification of artificial sRNA sequences inducing resistance to any of the multiple viruses infecting *N. benthamiana*. More generally, the application of such methodology should definitely accelerate the generation of plants with enhanced, durable antiviral resistance to ensure food security in the near future.

## MATERIALS AND METHODS

### TSWV Isolates

Twenty-nine, 65 and 61 complete sequences corresponding to TSWV segments L, M and S, respectively, were collected from the NCBI Nucleotide database (https://www.ncbi.nlm.nih.gov/nucleotide/). FASTA sequences of all segments for all isolates are included in Supplementary Text S1. The most relevant information regarding TSWV isolates used in P-SAMS-based amiRNA designs or in infection assays is included in Supplementary Table S1.

### Entropy Analyses

Clustal Omega (https://www.ebi.ac.uk/Tools/msa/clustalo/) with default parameters was used to independently align all the sequences of each segment. The Shannon entropy value of each position was calculated using the equation E = ((log2(freqA) x freqA) + (log2(freqC) x freqC) + (log2(freqG) x freqG) + (log2(freqT) x freqT)) x (-1), where “E” is “Entropy”, and “freqA”, “freqC”, “freqG” and “freqT” are the frequency of adenine, cytosine, guanine and thymine, respectively, at this particular position (with gaps being considered as elements of

variation). Finally, target site entropy was calculated as the sum of individual entropies of each target site position.

**Artificial Small RNA Design**

An updated version of the *P-SAMS* script (https://github.com/carringtonlab/p-sams) returning unlimited optimal results was used to retrieve the complete list of optimal amiRNAs targeting TSWV L, M or S segments. Input sequences used in amiRNA designs are included in Supplementary Text S2. The off-targeting filtering in *S. lycopersicum* transcriptome iTAGv2.3 (ftp://ftp.solgenomics.net/tomato_genome/annotation/ITAG2.3_release/) was enabled in all amiRNA designs. *TargetFinder* (Fahlgren et al. 2010) script (https://github.com/carringtonlab/TargetFinder) was ran to confirm that selected amiRNAs do not target significantly *N. benthamiana* transcriptome v5.1 (http://sefapps02.qut.edu.au/benWeb/subpages/downloads.php) (Nakasugi et al., 2014) (Supplementary Dataset S4).

**DNA Constructs**

Artificial sRNA constructs were generated following the methodology previously described (Carbonell et al., 2014) and using the oligonucleotides output by P-SAMS. AmiRNA constructs *35S:amiR-TSWV-L-1*, *35S:amiR-TSWV-L-2*, *35S:amiR-TSWV-L-3, 35S:amiR-TSWV-L-4*, *35S:amiR-TSWV-L-5, 35S:amiR-TSWV-M-1*, *35S:amiR-TSWV-M-2*, *35S:amiR-TSWV-M-3, 35S:amiR-TSWV-M-4*, *35S:amiR-TSWV-M-5, 35S:amiR-TSWV-S-1*, *35S:amiR-TSWV-S-2*, *35S:amiR-TSWV-S-3, 35S:amiR-TSWV-S-4*, *35S:amiR-TSWV-S-5,* were obtained by ligating annealed oligo pairs D2127/D2128, D2129/D2130, D2131/D2132, D2133/D2134, D2135/D2136, D2137/D2138, D2139/D2140, D2141/D2142, D2143/D2144, D2145/D2146, D2147/D2148, D2149/D2150 D2151/D2152, D2153/D2154 and D2155/D2156, respectively, into *pMDC32B-AtMIR390a-B/c* (Addgene plasmid #51776) (Carbonell et al., 2014). Syn-tasiRNA constructs *35S:syn-tasiR-TSWV* and *35S:syn-tasiR-GUS* were obtained by ligating annealed oligo pairs AC-45/AC-46 and AC-47/AC-48, respectively, into *pMDC32B-AtTAS1c-*

*B/c* (Addgene plasmid #51773) (Carbonell et al., 2014). DNA oligonucleotides used to generate the artificial sRNA constructs are listed in Supplementary Table S3.

*35S:amiR-GUS-1* and *35S:amiR-GUS-2*, *35S:GUS* and *35S:MIR173a* constructs were described before (Montgomery et al., 2008a; Carbonell and Daros, 2017).

**Plant Bioassays and TSWV Inoculation**

*N. benthamiana* plants were grown in a growth chamber at 25ºC with a 12 h-light/12 h-dark photoperiod. For each TSWV isolate, a crude extract from *N. benthamiana* infected tissue was used as inoculum and applied to the whole surface of the third true leaf of three weeks old plants as described (Carbonell and Daros, 2018). In artificial sRNA-based functional assays, this third leaf was agroinfiltrated two days before with cultures of *A. tumefaciens* GV3101 as described (Cuperus et al., 2010; Carbonell et al., 2012).

**RNA Gel Blot Assays**

Total RNA from *N. benthamiana* leaves was isolated using TRIzol reagent (Thermo Fisher Scientific) followed by chloroform extraction. RNA was precipitated with an equal volume of isopropanol for 20 min. Triplicate samples from two infiltrated leaves each were analyzed. RNA gel blot assays were done as described (Montgomery et al., 2008b; Cuperus et al., 2010). Briefly, 20 µg of total RNA were resolved by denaturing PAGE in 17% polyacrylamide gels containing 0.5xTBE and 7 M urea, and transferred to a positively-charged nylon membrane. Northern blot hybridizations were done at 40ºC in the presence of PerfectHyb Plus Hybridization Buffer (Sigma-Aldrich) with DNA probes end-labeled using [$\gamma$-$^{32}$P]ATP and T4 polynucleotide kinase (Thermo Fisher Scientific). A Fujifilm FLA-5100 imaging system was used to measure blot hybridization signals (photostimulated luminescence). DNA oligonucleotides used as probes are listed in Supplementary Table S4.

### DAS-ELISA Assays

TSWV accumulation in extracts from apical leaves collected at 10 or 20 dpi were analyzed by double antibody sandwich enzyme-linked immunosorbent assay (DAS-ELISA) using the TSWV Complete kit (Bioreba) essentially as indicated by the manufacturer. Briefly, samples were homogenized in extraction buffer at a 1:50 dilution and two technical replicates of 0.1 mL of extract were analyzed. The absorbance of each sample was measured at 405 nm using a model 550 Microplate Reader (Bio-Rad). Samples were considered to be infected (DAS-ELISA-positive) when absorbance was higher than three times the average absorbance of the samples from non TSWV-inoculated controls. The absorbance values were used as an indirect estimate of the viral accumulation as reported previously (Soler-Aleixandre et al., 2007).

## ACKNOWLEDGEMENTS

We thank Verónica Aragonés for invaluable technical assistance and Dr. Javier Forment for helping with the entropy analyses. This study was supported by grants BIO2014-54269-R and BIO2017-83184-R from Ministerio de Ciencia, Innovación y Universidades (Spain; cofounded FEDER funds) to J.-A.D., and by grant RTA2013-00047-C02-02 from Instituto Nacional de Investigaciones Agrarias (INIA; cofounded FEDER funds) to C.L.. A.C. was the recipient of an Individual Fellowship from the European Union's Horizon 2020 research and innovation programme under the Marie Sklodowska Curie grant agreement No. 655841, and was selected in the Ramón y Cajal programme (RYC-2017-21648) from Ministerio de Ciencia, Innovación y Universidades (Spain).

## AUTHOR-RECOMMENDED INTERNET RESOURCES

Clustal Omega multiple sequence alignment program:
https://www.ebi.ac.uk/Tools/msa/clustalo/
National Center for Biotechnology Information (NCBI) Nucleotide database:
https://www.ncbi.nlm.nih.gov/nucleotide/
P-SAMS website: http://p-sams.carringtonlab.org/

P-SAMS software: https://github.com/carringtonlab/p-sams

TargetFinder software: https://github.com/carringtonlab/TargetFinder

## FIGURE LEGENDS

**Fig. 1.** Diagram of the steps for the design and synthesis of anti-TSWV amiRNAs and syn-tasiRNAs, and for the analysis of their antiviral activity. Each step is described in light grey boxes. The product of each step is shown in light blue boxes.

**Fig. 2**. Analysis of TSWV nucleotidic variability. **A,** Entropy profiles of TSWV segments L, M and S. **B,** Entropy profiles of target sites from selected amiRNAs.

**Fig. 3.** Localization of amiRNA target sites in TSWV genomic and antigenomic RNAs. Approximate amiRNA cleavage site position in L, M and S segments is indicated with blue, green and orange arrows, respectively. Top right, the meaning of other shapes is indicated in a box. vRNA, viral RNA; vcRNA, viral complementary RNA.

**Fig. 4.** Analysis of the antiviral activity of several artificial microRNAs (amiRNAs) targeting TSWV L segment RNAs. **A,** Base pairing of amiRNAs and target TSWV-PVR RNAs. Anti-TSWV amiRNA and TSWV-PVR-L sequences are shown in blue and black, respectively. Coordinates of the complete target site in TSWV-PVR-L RNAs are given. The colored arrows indicate the amiRNA-predicted cleavage site. **B**, Photos at 7 days post-inoculation (dpi) of agroinfiltrated leaves further inoculated with TSWV-PVR. **C,** Bar graph showing the mean number ($n$ = 6) + standard deviation (SD) of local lesions in indicated samples at 7 dpi. **D,** Photos at 10 dpi of sets of 3 plants agroinfiltrated and further inoculated with TSWV-PVR as indicated. TSWV-induced characteristic symptoms of leaf chlorosis and epinasty are pointed with an arrow. **E,** 2-D line graph showing, for each six-plant set listed in the box, the percentage of symptomatic plants per day during 20 dpi. **F,** Bar graph representing the mean ($n$ = 6) + standard deviation (SD) absorbance obtained in DAS-ELISA assays on indicated samples collected at 10 dpi, as an indirect estimate of TSWV accumulation. Bars with the letters “a” and “b” are statistically significantly different from that of sample *35S:amiR-GUS-1* + TSWV-PVR and *35S:amiR-GUS-2* + TSWV-PVR, respectively ($P$ < 0.05 in pair-wise Student’s t-test comparisons).

**Fig. 5.** Analysis of the antiviral activity of several amiRNAs targeting TSWV M segment RNAs. **A,** Base pairing of amiRNAs and target TSWV-PVR RNAs. Anti-

TSWV amiRNA and TSWV-PVR-M sequences are shown in green and black, respectively. Other details are as in Fig. 4A. **B-F** labels are the same as in Fig. 4B-F.

**Fig. 6.** Analysis of the antiviral activity of several amiRNAs targeting TSWV S segment RNAs. **A,** Base pairing of amiRNAs and target TSWV-PVR RNAs. Anti-TSWV amiRNA and TSWV-PVR-S sequences are shown in orange and black, respectively. Other details are as in Fig. 4A. **B-F** labels are the same as in Fig. 4B-F.

**Fig. 7.** Analysis of the antiviral activity of synthetic *trans*-acting small interfering RNAs (syn-tasiRNAs) targeting TSWV RNAs. **A,** Organization of syn-tasiRNA constructs. tasiRNA and syn-tasiRNA positions are indicated by grey and black brackets, respectively. Anti-TSWV syn-tasiRNA nucleotides are in purple, while anti-GUS syn-tasiRNA nucleotides are in black. Base pairing of syn-tasiRNAs and target TSWV-PVR RNAs is shown. Other details are the same as in Fig. 4A.

**B-F,** labels are the same as in Fig. 4B-F. Bars with the letter "a" are statistically significantly different from that of sample *35S:amiR-GUS-1* + *35S:MIR173a* + TSWV-PVR ($P < 0.05$ in pair-wise Student's t-test comparisons).

**Fig. 8.** Comparative analysis of the antiviral activity of artificial microRNAs (amiRNAs) and synthetic trans-acting small interfering RNAs (syn-tasiRNAs) against TSWV-PVR isolate. **A-E,** labels are the same as in Fig. 4B-4F. Bars with the letter "a" are statistically significantly different from that of sample *35S:GUS* + *35S:MIR173a* + TSWV-PVR ($P < 0.05$ in pair-wise Student's t-test comparisons).

**Fig. 9.** Comparative analysis of the antiviral activity of artificial microRNAs (amiRNAs) and synthetic trans-acting small interfering RNAs (syn-tasiRNAs) against TSWV-LL-N.05 isolate. **A-E,** labels are the same as in Fig. 4B-4F. Bars with the letter "a" are statistically significantly different from that of sample *35S:GUS* + *35S:MIR173a* + TSWV-LL-N.05 ($P < 0.05$ in pair-wise Student's t-test comparisons).

**Table 1.** Relevant information of selected amiRNAs targeting TSWV segments L, M or S.

**Table 2.** Summary of results obtained from symptom and DAS-ELISA analyses in all bioassays.

## ELECTRONIC EXTRA

**Supplementary Dataset S1.** Complete list of optimal results generated by P-SAMS amiRNA Designer for the design of amiRNAs targeting segments L, M or S of 6 TSWV isolates with no off-targets in *Solanum lycopersicum*.

**Supplementary Dataset S2.** Shannon entropy value for each nucleotidic position in TSWV.

**Supplementary Dataset S3.** Target prediction (TP) score, target site (TS) entropy and other relevant information regarding all amiRNA optimal results obtained with P-SAMS amiRNA Designer.

**Supplementary Dataset S4.** *TargetFinder* results for selected amiRNAs in *N. benthamiana*.

**Supplementary Fig. S1.** Analysis of the infectivity in *N. benthamiana* of an extract obtained from plants infected with TSWV-PVR. The 2-D line graph shows, for each 12-plant set listed in the box, the percentage of symptomatic plants per day during 20 dpi.

**Supplementary Fig. S2**. Comparative analysis of the accumulation of anti-GUS and anti-TSWV amiRNAs in *Nicotiana benthamiana* agroinfiltrated leaves. Bars in grey, blue, green and orange show the photostimulated luminescence mean signal (n = 3 + SD) corresponding to anti-GUS, anti-TSWV-L, anti-TSWV-M or anti-TSWV-S amiRNA species, respectively, detected by Northern blot. In each case, the mean value was calculated relative to that of the amiRNA with higher value.

**Supplementary Fig. S3.** Analysis of the infectivity *N. benthamiana* of an extract obtained from plants infected with TSWV-LL-N.05. Other details are the same as in Supplementary Fig. S1.

**Supplementary Fig. S4**. Comparative analysis of the accumulation of anti-GUS and anti-TSWV syn-tasiRNAs, and of amiR-TSWV-L-5 amiRNA in *Nicotiana benthamiana* agroinfiltrated leaves. Bars in grey, blue, violet, and gold show the photostimulated luminescence mean signal (n = 3 + SD) corresponding to syn-

tasiR-GUS, amiR-TSWV-L-5, syn-tasiR-TSWV and miR173a, respectively, detected by Northern blot. In each case, the mean value was calculated relative to that of the sRNA with higher value.

**Supplementary Table S1.** Relevant information regarding TSWV isolates used this study in P-SAMS-based amiRNA designs or in infection assays.

**Supplementary Table S2.** Possible *N. benthamiana* off-targets of selected amiRNAs based on *TargetFinder* target prediction.

**Supplementary Table S3.** Name, sequence and use of DNA oligonucleotides used in this study.

**Supplementary Table S4.** DNA oligonucleotides used to generate probes for Northern blot assays.

**Supplementary Text S1.** DNA sequences in FASTA format of all TSWV isolates collected from the NCBI Nucleotide database.

**Supplementary Text S2.** DNA sequences in FASTA format used in P-SAMS-based amiRNA designs.

**Supplementary Text S3.** DNA sequence in FASTA format of all artificial small RNA generating precursors used in this study.

## LITERATURE CITED

Brousse, C., Liu, Q., Beauclair, L., Deremetz, A., Axtell, M.J., and Bouche, N. 2014. A non-canonical plant microRNA target site. Nucleic Acids Res 42:5270-5279.

Bucher, E., Lohuis, D., van Poppel, P.M., Geerts-Dimitriadou, C., Goldbach, R., and Prins, M. 2006. Multiple virus resistance at a high frequency using a single transgene construct. J Gen Virol 87:3697-3701.

Carbonell, A. 2017a. Artificial small RNA-based strategies for effective and specific gene silencing in plants. Pages 110-127 in: Plant Gene Silencing: Mechanisms and Applications, T. Dalmay, ed. CABI Publishing.

Carbonell, A. 2017b. Plant ARGONAUTEs: Features, Functions, and Unknowns. Methods Mol Biol 1640:1-21.

Carbonell, A. 2018. Design and High-Throughput Generation of Artificial Small RNA Constructs for Plants. Methods Mol Biol (in press).

Carbonell, A., and Daros, J.A. 2017. Artificial microRNAs and synthetic trans-acting small interfering RNAs interfere with viroid infection. Mol Plant Pathol 18:746-753.

Carbonell, A., and Daros, J.A. 2018. Design, Synthesis and Functional Analysis of Highly Specific Artificial Small RNAs With Antiviral Activity in Plants. Methods Mol Biol (in press).

Carbonell, A., Carrington, J.C., and Daros, J.A. 2016. Fast-forward generation of effective artificial small RNAs for enhanced antiviral defense in plants. RNA Dis 3:e 1130.

Carbonell, A., Takeda, A., Fahlgren, N., Johnson, S.C., Cuperus, J.T., and Carrington, J.C. 2014. New generation of artificial MicroRNA and synthetic trans-acting small interfering RNA vectors for efficient gene silencing in Arabidopsis. Plant Physiol 165:15-29.

Carbonell, A., Fahlgren, N., Mitchell, S., Cox, K.L., Jr., Reilly, K.C., Mockler, T.C., and Carrington, J.C. 2015. Highly specific gene silencing in a monocot species by artificial microRNAs derived from chimeric miRNA precursors. Plant J 82:1061-1075.

Carbonell, A., Fahlgren, N., Garcia-Ruiz, H., Gilbert, K.B., Montgomery, T.A., Nguyen, T., Cuperus, J.T., and Carrington, J.C. 2012. Functional analysis of three Arabidopsis ARGONAUTES using slicer-defective mutants. Plant Cell 24:3613-3629.

Chen, L., Cheng, X., Cai, J., Zhan, L., Wu, X., Liu, Q., and Wu, X. 2016. Multiple virus resistance using artificial trans-acting siRNAs. J Virol Methods 228:16-20.

Cuperus, J.T., Carbonell, A., Fahlgren, N., Garcia-Ruiz, H., Burke, R.T., Takeda, A., Sullivan, C.M., Gilbert, S.D., Montgomery, T.A., and Carrington, J.C. 2010. Unique functionality of 22-nt miRNAs in triggering RDR6-dependent siRNA biogenesis from target transcripts in Arabidopsis. Nat Struct Mol Biol 17:997-1003.

de la Luz Gutierrez-Nava, M., Aukerman, M.J., Sakai, H., Tingey, S.V., and Williams, R.W. 2008. Artificial trans-acting siRNAs confer consistent and effective gene silencing. Plant Physiol 147:543-551.

Debreczeni, D.E., Lopez, C., Aramburu, J., Daros, J.A., Soler, S., Galipienso, L., Falk, B.W., and Rubio, L. 2015. Complete sequence of three different biotypes of tomato spotted wilt virus (wild type, tomato Sw-5 resistance-breaking and pepper Tsw resistance-breaking) from Spain. Arch Virol 160:2117-2123.

Fahim, M., Millar, A.A., Wood, C.C., and Larkin, P.J. 2012. Resistance to Wheat streak mosaic virus generated by expression of an artificial polycistronic microRNA in wheat. Plant Biotechnol J 10:150-163.

Fahlgren, N., and Carrington, J.C. 2010. miRNA Target Prediction in Plants. Methods Mol Biol 592:51-57.

Fahlgren, N., Hill, S.T., Carrington, J.C., and Carbonell, A. 2016. P-SAMS: a web site for plant artificial microRNA and synthetic trans-acting small interfering RNA design. Bioinformatics 32:157-158.

Goodin, M.M., Zaitlin, D., Naidu, R.A., and Lommel, S.A. 2008. Nicotiana benthamiana: its history and future as a model for plant-pathogen interactions. Mol Plant Microbe Interact 21:1015-1026.

Jan, F.J., Fagoaga, C., Pang, S.Z., and Gonsalves, D. 2000. A minimum length of N gene sequence in transgenic plants is required for RNA-mediated tospovirus resistance. J Gen Virol 81:235-242.

Kis, A., Tholt, G., Ivanics, M., Varallyay, E., Jenes, B., and Havelda, Z. 2016. Polycistronic artificial miRNA-mediated resistance to Wheat dwarf virus in barley is highly efficient at low temperature. Mol Plant Pathol 17:427-437.

Kormlink, R. 2011. The molecular biology of tospoviruses and resistance strategies. Pages 163-191 in: Bunyaviridae: Molecular and Cellular Biology, R.M. Elliot and A. Plyusin, eds. Plenum Press, New York.

Kung, Y.J., Lin, S.S., Huang, Y.L., Chen, T.C., Harish, S.S., Chua, N.H., and Yeh, S.D. 2012. Multiple artificial microRNAs targeting conserved motifs of the replicase

gene confer robust transgenic resistance to negative-sense single-stranded RNA plant virus. Mol Plant Pathol 13:303-317.

Lafforgue, G., Martinez, F., Niu, Q.W., Chua, N.H., Daros, J.A., and Elena, S.F. 2013. Improving the effectiveness of artificial microRNA (amiR)-mediated resistance against Turnip mosaic virus by combining two amiRs or by targeting highly conserved viral genomic regions. J Virol 87:8254-8256.

Lafforgue, G., Martinez, F., Sardanyes, J., de la Iglesia, F., Niu, Q.W., Lin, S.S., Sole, R.V., Chua, N.H., Daros, J.A., and Elena, S.F. 2011. Tempo and mode of plant RNA virus escape from RNA interference-mediated resistance. J Virol 85:9686-9695.

Lin, S.S., Wu, H.W., Elena, S.F., Chen, K.C., Niu, Q.W., Yeh, S.D., Chen, C.C., and Chua, N.H. 2009. Molecular evolution of a viral non-coding sequence under the selective pressure of amiRNA-mediated silencing. PLoS Pathog 5:e1000312.

Liu, Q., Wang, F., and Axtell, M.J. 2014. Analysis of complementarity requirements for plant microRNA targeting using a Nicotiana benthamiana quantitative transient assay. Plant Cell 26:741-753.

Liu, S.R., Zhou, J.J., Hu, C.G., Wei, C.L., and Zhang, J.Z. 2017. MicroRNA-Mediated Gene Silencing in Plant Defense and Viral Counter-Defense. Front Microbiol 8:1801.

MacKenzie, D.J., and Ellis, P.J. 1992. Resistance to tomato spotted wilt virus infection in transgenic tobacco expressing the viral nucleocapsid gene. Mol Plant Microbe Interact 5:34-40.

Mitter, N., Zhai, Y., Bai, A.X., Chua, K., Eid, S., Constantin, M., Mitchell, R., and Pappu, H.R. 2016. Evaluation and identification of candidate genes for artificial

microRNA-mediated resistance to tomato spotted wilt virus. Virus Res 211:151-158.

Montgomery, T.A., Howell, M.D., Cuperus, J.T., Li, D., Hansen, J.E., Alexander, A.L., Chapman, E.J., Fahlgren, N., Allen, E., and Carrington, J.C. 2008a. Specificity of ARGONAUTE7-miR390 interaction and dual functionality in TAS3 trans-acting siRNA formation. Cell 133:128-141.

Montgomery, T.A., Yoo, S.J., Fahlgren, N., Gilbert, S.D., Howell, M.D., Sullivan, C.M., Alexander, A., Nguyen, G., Allen, E., Ahn, J.H., and Carrington, J.C. 2008b. AGO1-miR173 complex initiates phased siRNA formation in plants. Proc Natl Acad Sci U S A 105:20055-20062.

Nakasugi, K., Crowhurst, R., Bally, J., and Waterhouse, P. 2014. Combining transcriptome assemblies from multiple de novo assemblers in the allo-tetraploid plant Nicotiana benthamiana. PLoS One 9:e91776.

Niu, Q.W., Lin, S.S., Reyes, J.L., Chen, K.C., Wu, H.W., Yeh, S.D., and Chua, N.H. 2006. Expression of artificial microRNAs in transgenic Arabidopsis thaliana confers virus resistance. Nat Biotechnol 24:1420-1428.

Ossowski, S., Schwab, R., and Weigel, D. 2008. Gene silencing in plants using artificial microRNAs and other small RNAs. Plant J 53:674-690.

Peng, J.C., Chen, T.C., Raja, J.A., Yang, C.F., Chien, W.C., Lin, C.H., Liu, F.L., Wu, H.W., and Yeh, S.D. 2014. Broad-spectrum transgenic resistance against distinct tospovirus species at the genus level. PLoS One 9:e96073.

Plyusnin, A., Beaty, B., Elliot, R., Goldbach, R., Kormelink, R., Lundkvist, A., Schmaljohn, C., and Tesh, R. 2012. Bunyaviridae. Pages 725-741 in: Virus

taxonomy: ninth report of the International Commitee on Taxonomy ov Viruses, A.M.Q. King, M.J. Adams, E.B. Carsyens, and E.J. Lefkowitz, eds. Elsevier Academic Press, London.

Pooggin, M.M. 2017. RNAi-mediated resistance to viruses: a critical assessment of methodologies. Curr Opin Virol 26:28-35.

Prins, M., Resende Rde, O., Anker, C., van Schepen, A., de Haan, P., and Goldbach, R. 1996. Engineered RNA-mediated resistance to tomato spotted wilt virus is sequence specific. Mol Plant Microbe Interact 9:416-418.

Scholthof, K.B., Adkins, S., Czosnek, H., Palukaitis, P., Jacquot, E., Hohn, T., Hohn, B., Saunders, K., Candresse, T., Ahlquist, P., Hemenway, C., and Foster, G.D. 2011. Top 10 plant viruses in molecular plant pathology. Mol Plant Pathol 12:938-954.

Schwab, R., Ossowski, S., Warthmann, N., and Weigel, D. 2010. Directed gene silencing with artificial microRNAs. Methods Mol Biol 592:71-88.

Schwab, R., Ossowski, S., Riester, M., Warthmann, N., and Weigel, D. 2006. Highly specific gene silencing by artificial microRNAs in Arabidopsis. Plant Cell 18:1121-1133.

Shannon, C.E. 1997. The mathematical theory of communication. MD Comput 14:306-317.

Sherwood, J.L., German, T.L., Moyer, J.W., and D.E., U. 2003. Tomato spotted wilt. The Plant Health Instructor.

Soler-Aleixandre, S., López, C., Cebolla-Cornejo, J., and Nuez, F. 2007. Sources of Resistance to Pepino mosaic virus (PepMV) in Tomato. HortScience 42:40-45.

Sonoda, S., and Tsumuki, H. 2004. Analysis of RNA-mediated virus resistance by NSs and NSm gene sequences from Tomato spotted wilt virus. Plant Sci 166:771-778.

Turina, M., Kormelink, R., and Resende, R.O. 2016. Resistance to Tospoviruses in Vegetable Crops: Epidemiological and Molecular Aspects. Annu Rev Phytopathol 54:347-371.

Watson, J.M., Fusaro, A.F., Wang, M., and Waterhouse, P.M. 2005. RNA silencing platforms in plants. FEBS Lett 579:5982-5987.

Whitfield, A.E., Ullman, D.E., and German, T.L. 2005. Tospovirus-thrips interactions. Annu Rev Phytopathol 43:459-489.

Yu, S., and Pilot, G. 2014. Testing the efficiency of plant artificial microRNAs by transient expression in Nicotiana benthamiana reveals additional action at the translational level. Front Plant Sci 5:622.

**Table 1.** Relevant information of selected amiRNAs targeting TSWV segments L, M or S.

| amiRNA name | amiRNA sequence | TP score[a] | TS entropy[b] | Target fragment (TS coordinates) |
|---|---|---|---|---|
| amiR-TSWV-L1 | UGCUUAAAAUCGUUGUUACCA | 1 | 0 | L (9-29) |
| amiR-TSWV-L2 | UGUCCUGCUAAGAACAUUCCA | 1 | 0.22 | L (7760-7780) |
| amiR-TSWV-L3 | UCAGAGUGCACAAUCCAUCUU | 1 | 0.70 | L (4500-4520) |
| amiR-TSWV-L4 | UGGUAUACAAACCUUCUUCAU | 1 | 0.85 | L (4261-4281) |
| amiR-TSWV-L5 | UGUAAGACGUGAUUGUGUCCU | 1 | 1.17 | L (4061-4081) |
| amiR-TSWV-M1 | UAUCAGCUCUGGGUGAAUCGG | 1.42 | 0.50 | M (772-792) |
| amiR-TSWV-M2 | UUAAUAGUGAACACUAAGCUC | 1.50 | 1.07 | M (3459-3479) |
| amiR-TSWV-M3 | UUGGUAUAGUGGGGCAUACCG | 1.83 | 0.70 | M (508-528) |
| amiR-TSWV-M4 | UAGAACUAGUGGUAAAAGCGU | 2 | 0.11 | M (4730-4750) |
| amiR-TSWV-M5 | UAACCUUAAUCCAGACAUCUA | 2 | 0.54 | M (4813-4833) |
| amiR-TSWV-S1 | UUCAGACAGGAUUGGAGCCAA | 1.17 | 0.95 | S (2739-2759) |
| amiR-TSWV-S2 | UUGGGAGGUAGCUUACCUCUA | 1.50 | 0.76 | S (2549-2569) |
| amiR-TSWV-S3 | UGUACAGCCAUUCAUGGACAA | 1.50 | 1.01 | S (662-682) |
| amiR-TSWV-S4 | UAAGCCUAUGGAUUACCUCUA | 1.50 | 1.11 | S (2603-2623) |
| amiR-TSWV-S5 | UCUAAGGUUAAGCUCACUCAC | 2 | 0 | S (2981-3001) |

[a] TP score: target prediction score from TargetFinder analysis

[b] TS entropy: target site entropy.

**Table 2.** Summary of results obtained from symptom and DAS-ELISA analyses in all bioassays.

| | | Analysis at 10 dpi | | Analysis at 20 dpi | |
|---|---|---|---|---|---|
| **Sample** | **Figure** | **Symptomatic plants/Total** | **DAS-ELISA positive/Total** | **Symptomatic plants/Total** | **DAS-ELISA positive/Total** |
| *35S:GUS* | 4 | 0/6 | 0/6 | 0/6 | 0/6 |
| *35S:amiR-GUS-1* + TSWV-PVR | 4 | 6/6 | 6/6 | 6/6 | 6/6 |
| *35S:amiR-GUS-2* + TSWV-PVR | 4 | 6/6 | 6/6 | 6/6 | 6/6 |
| *35S:amiR-TSWV-L-1* + TSWV-PVR | 4 | 6/6 | 6/6 | 6/6 | 6/6 |
| *35S:amiR-TSWV-L-2* + TSWV-PVR | 4 | 6/6 | 6/6 | 6/6 | 6/6 |
| *35S:amiR-TSWV-L-3* + TSWV-PVR | 4 | 6/6 | 6/6 | 6/6 | 6/6 |
| *35S:amiR-TSWV-L-4* + TSWV-PVR | 4 | 3/6 | 3/6 | 3/6 | 3/6 |
| *35S:amiR-TSWV-L-5* + TSWV-PVR | 4 | 0/6 | 0/6 | 0/6 | 0/6 |
| *35S:GUS* | 5 | 0/6 | 0/6 | 0/6 | 0/6 |
| *35S:amiR-GUS-1* + TSWV-PVR | 5 | 6/6 | 6/6 | 6/6 | 6/6 |
| *35S:amiR-GUS-2* + TSWV-PVR | 5 | 6/6 | 6/6 | 6/6 | 6/6 |
| *35S:amiR-TSWV-M-1* + TSWV-PVR | 5 | 0/6 | 0/6 | 1/6 | 1/6 |
| *35S:amiR-TSWV-M-2* + TSWV-PVR | 5 | 6/6 | 6/6 | 6/6 | 6/6 |
| *35S:amiR-TSWV-M-3* + TSWV-PVR | 5 | 2/6 | 2/6 | 3/6 | 3/6 |

| | | | | | |
|---|---|---|---|---|---|
| *35S:amiR-TSWV-M-4* + TSWV-PVR | 5 | 6/6 | 6/6 | 6/6 | 6/6 |
| *35S:amiR-TSWV-M-5* + TSWV-PVR | 5 | 6/6 | 6/6 | 6/6 | 6/6 |
| *35S:GUS* | 6 | 0/6 | 0/6 | 0/6 | 0/6 |
| *35S:amiR-GUS-1* + TSWV-PVR | 6 | 6/6 | 6/6 | 6/6 | 6/6 |
| *35S:amiR-GUS-2* + TSWV-PVR | 6 | 6/6 | 6/6 | 6/6 | 6/6 |
| *35S:amiR-TSWV-S-1* + TSWV-PVR | 6 | 6/6 | 6/6 | 6/6 | 6/6 |
| *35S:amiR-TSWV-S-2* + TSWV-PVR | 6 | 6/6 | 6/6 | 6/6 | 6/6 |
| *35S:amiR-TSWV-S-3* + TSWV-PVR | 6 | 6/6 | 6/6 | 6/6 | 6/6 |
| *35S:amiR-TSWV-S-4* + TSWV-PVR | 6 | 6/6 | 6/6 | 6/6 | 6/6 |
| *35S:amiR-TSWV-S-5* + TSWV-PVR | 6 | 6/6 | 6/6 | 6/6 | 6/6 |
| *35S:GUS* | 7 | 0/6 | 0/6 | 0/6 | 0/6 |
| *35S:syn-tasiR-GUS* + *35S:MIR173* + TSWV-PVR | 7 | 6/6 | 6/6 | 6/6 | 6/6 |
| *35S:syn-tasiR-TSWV* + *35S:GUS* + TSWV-PVR | 7 | 6/6 | 6/6 | 6/6 | 6/6 |
| *35S:syn-tasiR-TSWV* + *35S:MIR173* + TSWV-PVR | 7 | 0/6 | 0/6 | 0/6 | 0/6 |
| *35S:GUS* | 8 | 0/12 | 0/12 | 0/12 | 0/12 |
| *35S:GUS* + *35S:MIR173* + TSWV-PVR | 8 | 12/12 | 12/12 | 12/12 | 12/12 |

| | | | | | |
|---|---|---|---|---|---|
| *35S:amiR-TSWV-L-5* + *35S:MIR173* + TSWV-PVR | 8 | 0/12 | 2/12 | 2/12 | 2/12 |
| *35S:syn-tasiR-TSWV* + *35S:MIR173* + TSWV-PVR | 8 | 1/12 | 2/12 | 2/12 | 2/12 |
| *35S:GUS* | 9 | 0/12 | 0/12 | 0/12 | 0/12 |
| *35S:GUS* + *35S:MIR173* + TSWV-LL-N.05 | 9 | 12/12 | 12/12 | 12/12 | 12/12 |
| *35S:amiR-TSWV-L-5* + *35S:MIR173* + TSWV-LL-N.05 | 9 | 0/12 | 2/12 | 5/12 | 5/12 |
| *35S:syn-tasiR-TSWV* + *35S:MIR173* + TSWV-LL-N.05 | 9 | 0/12 | 1/12 | 3/12 | 3/12 |

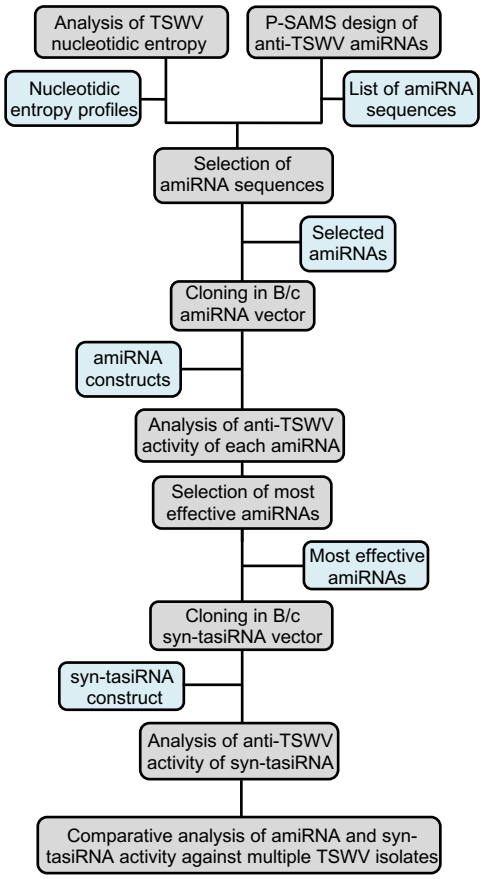
Analysis of TSWV nucleotidic entropy
P-SAMS design of anti-TSWV amiRNAs
Nucleotidic entropy profiles
List of amiRNA sequences
Selection of amiRNA sequences
Selected amiRNAs
Cloning in B/c amiRNA vector
amiRNA constructs
Analysis of anti-TSWV activity of each amiRNA
Selection of most effective amiRNAs
Most effective amiRNAs
Cloning in B/c syn-tasiRNA vector
syn-tasiRNA construct
Analysis of anti-TSWV activity of syn-tasiRNA
Comparative analysis of amiRNA and syn-tasiRNA activity against multiple TSWV isolates

**FIGURE 1**

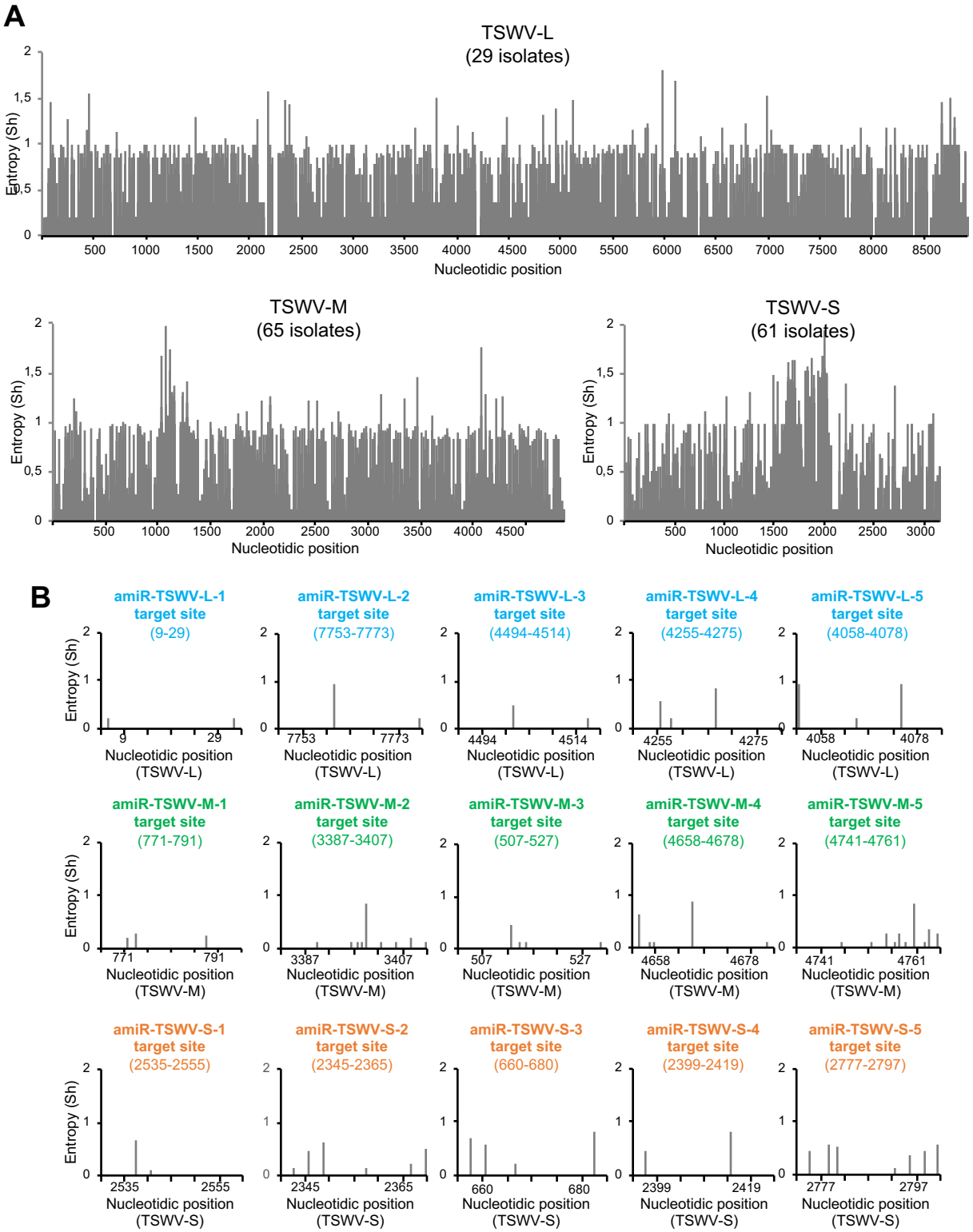
A
TSWV-L
(29 isolates)
Entropy (Sh)
Nucleotidic position
TSWV-M
(65 isolates)
TSWV-S
(61 isolates)
B
amiR-TSWV-L-1 target site (9-29)
amiR-TSWV-L-2 target site (7753-7773)
amiR-TSWV-L-3 target site (4494-4514)
amiR-TSWV-L-4 target site (4255-4275)
amiR-TSWV-L-5 target site (4058-4078)
amiR-TSWV-M-1 target site (771-791)
amiR-TSWV-M-2 target site (3387-3407)
amiR-TSWV-M-3 target site (507-527)
amiR-TSWV-M-4 target site (4658-4678)
amiR-TSWV-M-5 target site (4741-4761)
amiR-TSWV-S-1 target site (2535-2555)
amiR-TSWV-S-2 target site (2345-2365)
amiR-TSWV-S-3 target site (660-680)
amiR-TSWV-S-4 target site (2399-2419)
amiR-TSWV-S-5 target site (2777-2797)
Nucleotidic position (TSWV-L)
Nucleotidic position (TSWV-M)
Nucleotidic position (TSWV-S)

**FIGURE 2**

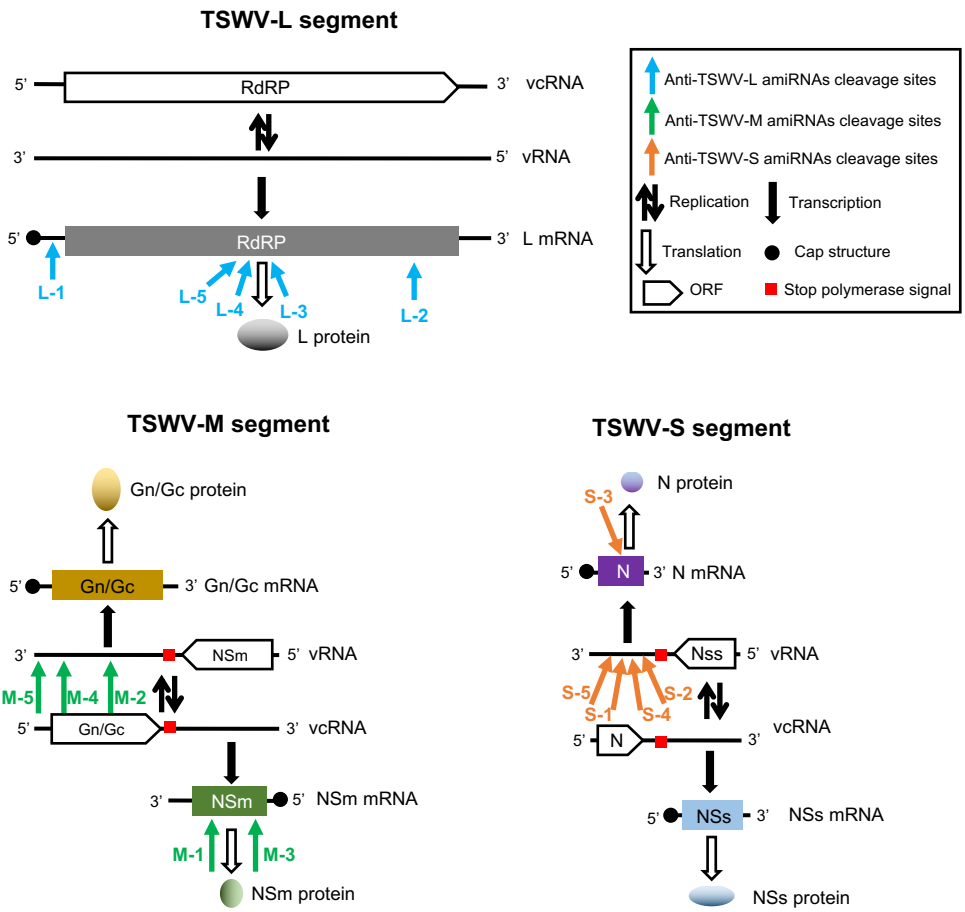
TSWV-L segment
5'
RdRP
3'
vcRNA
3'
5'
vRNA
5'
RdRP
3'
L mRNA
L-1
L-5
L-4
L-3
L-2
L protein
Anti-TSWV-L amiRNAs cleavage sites
Anti-TSWV-M amiRNAs cleavage sites
Anti-TSWV-S amiRNAs cleavage sites
Replication
Transcription
Translation
Cap structure
ORF
Stop polymerase signal
TSWV-M segment
Gn/Gc protein
5'
Gn/Gc
3'
Gn/Gc mRNA
3'
NSm
5'
vRNA
M-5
M-4
M-2
5'
Gn/Gc
3'
vcRNA
3'
NSm
5'
NSm mRNA
M-1
M-3
NSm protein
TSWV-S segment
N protein
S-3
5'
N
3'
N mRNA
3'
Nss
5'
vRNA
S-5
S-1
S-4
S-2
5'
N
3'
vcRNA
5'
NSs
3'
NSs mRNA
NSs protein

**FIGURE 3**

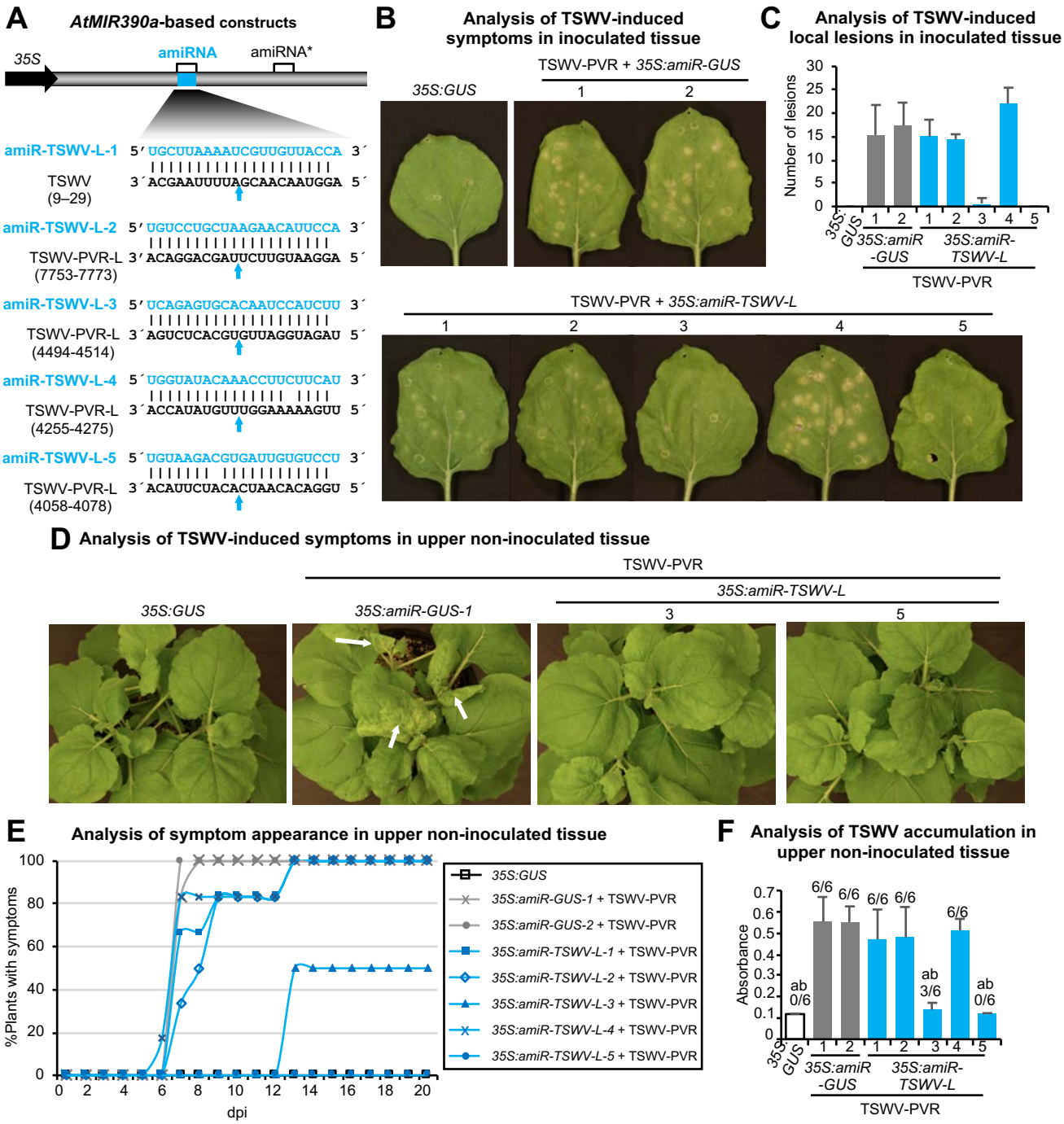
A
AtMIR390a-based constructs
35S
amiRNA
amiRNA*
amiR-TSWV-L-1 5′ UGCUUAAAAUCGUUGUUACCA 3′
TSWV (9–29) 3′ ACGAAUUUUAGCAACAAUGGA 5′
amiR-TSWV-L-2 5′ UGUCCUGCUAAGAACAUUCCA 3′
TSWV-PVR-L (7753-7773) 3′ ACAGGACGAUUCUUGUAAGGA 5′
amiR-TSWV-L-3 5′ UCAGAGUGCACAAUCCAUCUU 3′
TSWV-PVR-L (4494-4514) 3′ AGUCUCACGUGUUAGGUAGAU 5′
amiR-TSWV-L-4 5′ UGGUAUACAAACCUUCUUCAU 3′
TSWV-PVR-L (4255-4275) 3′ ACCAUAUGUUUGGAAAAAGUU 5′
amiR-TSWV-L-5 5′ UGUAAGACGUGAUUGUGUCCU 3′
TSWV-PVR-L (4058-4078) 3′ ACAUUCUACACUAACACAGGU 5′
B
Analysis of TSWV-induced symptoms in inoculated tissue
35S:GUS
TSWV-PVR + 35S:amiR-GUS
1
2
TSWV-PVR + 35S:amiR-TSWV-L
1
2
3
4
5
C
Analysis of TSWV-induced local lesions in inoculated tissue
Number of lesions
35S:GUS
35S:amiR-GUS
35S:amiR-TSWV-L
TSWV-PVR
D
Analysis of TSWV-induced symptoms in upper non-inoculated tissue
TSWV-PVR
35S:amiR-TSWV-L
35S:GUS
35S:amiR-GUS-1
3
5
E
Analysis of symptom appearance in upper non-inoculated tissue
%Plants with symptoms
dpi
35S:GUS
35S:amiR-GUS-1 + TSWV-PVR
35S:amiR-GUS-2 + TSWV-PVR
35S:amiR-TSWV-L-1 + TSWV-PVR
35S:amiR-TSWV-L-2 + TSWV-PVR
35S:amiR-TSWV-L-3 + TSWV-PVR
35S:amiR-TSWV-L-4 + TSWV-PVR
35S:amiR-TSWV-L-5 + TSWV-PVR
F
Analysis of TSWV accumulation in upper non-inoculated tissue
Absorbance
ab 0/6
6/6
6/6
6/6
6/6
ab 3/6
6/6
ab 0/6
35S:GUS
35S:amiR-GUS
35S:amiR-TSWV-L
TSWV-PVR

**FIGURE 4**

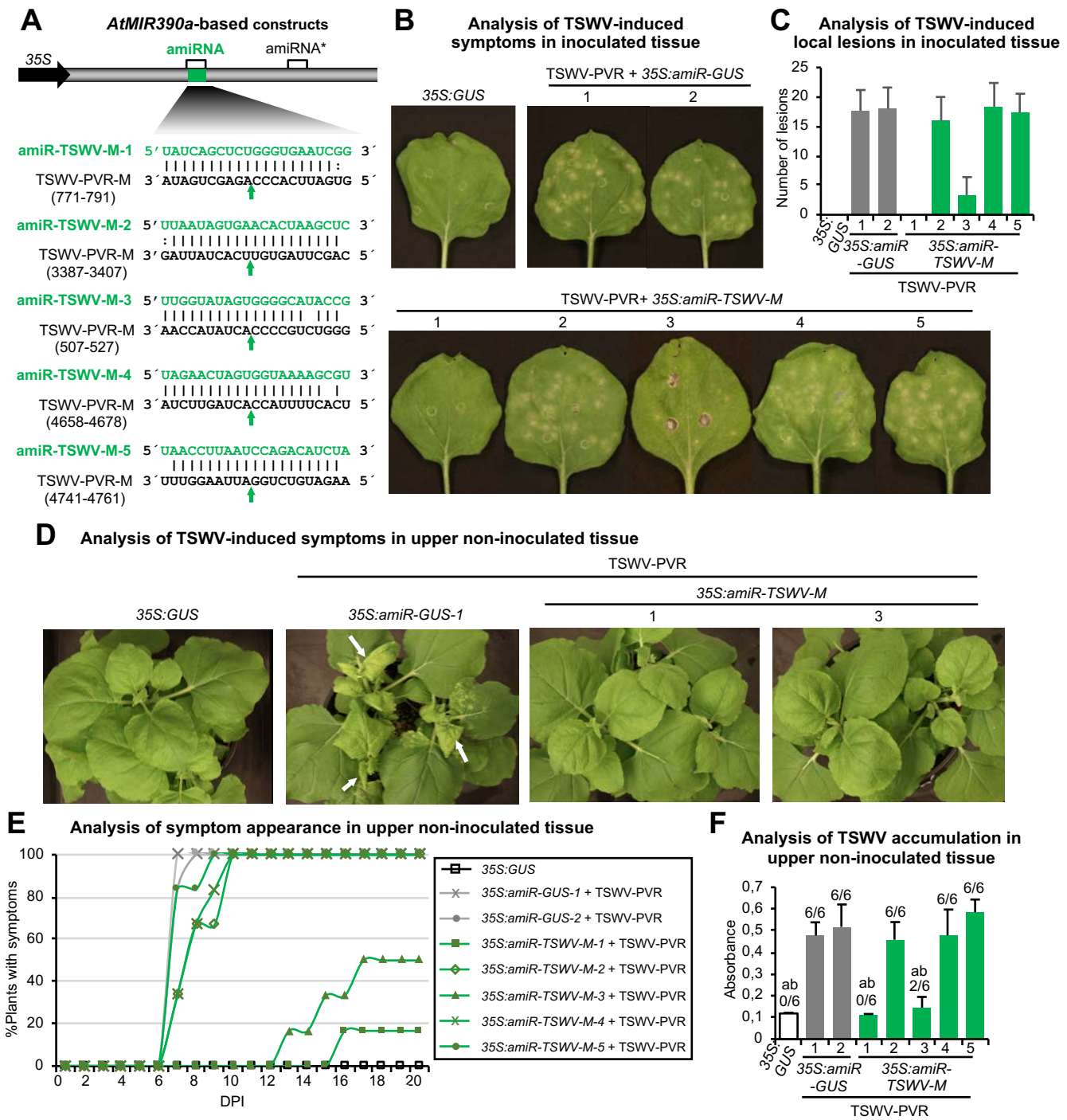
A
AtMIR390a-based constructs
35S
amiRNA
amiRNA*
amiR-TSWV-M-1 5′ UAUCAGCUCUGGGUGAAUCGG 3′
TSWV-PVR-M 3′ AUAGUCGAGACCCACUUAGUG 5′
(771-791)
amiR-TSWV-M-2 5′ UUAAUAGUGAACACUAAGCUC 3′
TSWV-PVR-M 3′ GAUUAUCACUUGUGAUUCGAC 5′
(3387-3407)
amiR-TSWV-M-3 5′ UUGGUAUAGUGGGGCAUACCG 3′
TSWV-PVR-M 3′ AACCAUAUCACCCCGUCUGGG 5′
(507-527)
amiR-TSWV-M-4 5′ UAGAACUAGUGGUAAAAGCGU 3′
TSWV-PVR-M 3′ AUCUUGAUCACCAUUUUCACU 5′
(4658-4678)
amiR-TSWV-M-5 5′ UAACCUUAAUCCAGACAUCUA 3′
TSWV-PVR-M 3′ UUUGGAAUUAGGUCUGUAGAA 5′
(4741-4761)
B
Analysis of TSWV-induced symptoms in inoculated tissue
35S:GUS
TSWV-PVR + 35S:amiR-GUS
1
2
TSWV-PVR+ 35S:amiR-TSWV-M
1
2
3
4
5
C
Analysis of TSWV-induced local lesions in inoculated tissue
Number of lesions
25
20
15
10
5
0
35S:GUS
1
2
35S:amiR-GUS
1
2
3
4
5
35S:amiR-TSWV-M
TSWV-PVR
D
Analysis of TSWV-induced symptoms in upper non-inoculated tissue
TSWV-PVR
35S:amiR-TSWV-M
35S:GUS
35S:amiR-GUS-1
1
3
E
Analysis of symptom appearance in upper non-inoculated tissue
%Plants with symptoms
100
80
60
40
20
0
0
2
4
6
8
10
12
14
16
18
20
DPI
35S:GUS
35S:amiR-GUS-1 + TSWV-PVR
35S:amiR-GUS-2 + TSWV-PVR
35S:amiR-TSWV-M-1 + TSWV-PVR
35S:amiR-TSWV-M-2 + TSWV-PVR
35S:amiR-TSWV-M-3 + TSWV-PVR
35S:amiR-TSWV-M-4 + TSWV-PVR
35S:amiR-TSWV-M-5 + TSWV-PVR
F
Analysis of TSWV accumulation in upper non-inoculated tissue
Absorbance
0,7
0,6
0,5
0,4
0,3
0,2
0,1
0
ab
0/6
6/6
6/6
ab
0/6
6/6
ab
2/6
6/6
6/6
35S:GUS
1
2
35S:amiR-GUS
1
2
3
4
5
35S:amiR-TSWV-M
TSWV-PVR

**FIGURE 5**

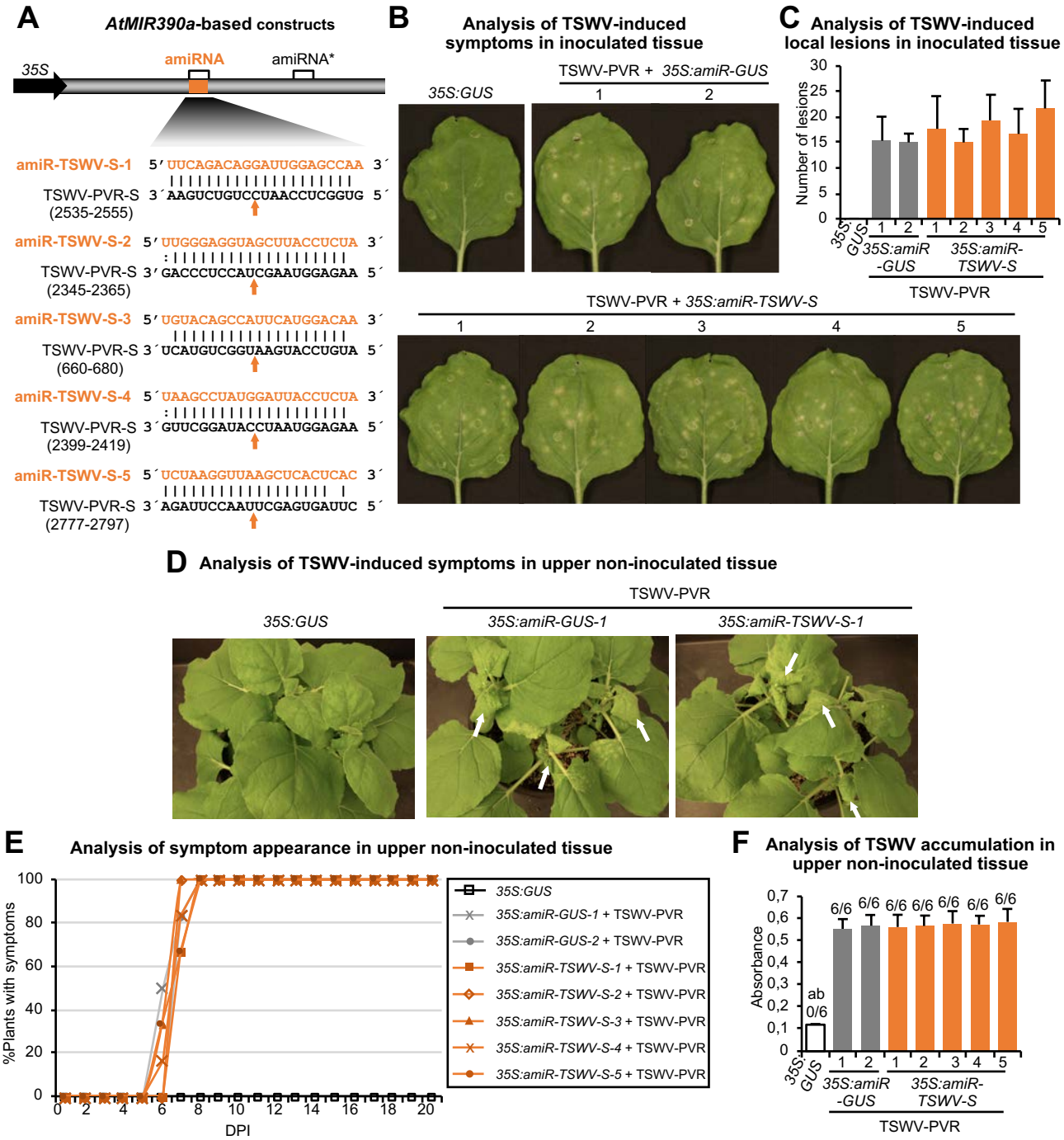
A
AtMIR390a-based constructs
35S
amiRNA
amiRNA*
amiR-TSWV-S-1 5′ UUCAGACAGGAUUGGAGCCAA 3′
TSWV-PVR-S 3′ AAGUCUGUCCUAACCUCGGUG 5′
(2535-2555)
amiR-TSWV-S-2 5′ UUGGGAGGUAGCUUACCUCUA 3′
TSWV-PVR-S 3′ GACCCUCCAUCGAAUGGAGAA 5′
(2345-2365)
amiR-TSWV-S-3 5′ UGUACAGCCAUUCAUGGACAA 3′
TSWV-PVR-S 3′ UCAUGUCGGUAAGUACCUGUA 5′
(660-680)
amiR-TSWV-S-4 5′ UAAGCCUAUGGAUUACCUCUA 3′
TSWV-PVR-S 3′ GUUCGGAUACCUAAUGGAGAA 5′
(2399-2419)
amiR-TSWV-S-5 5′ UCUAAGGUUAAGCUCACUCAC 3′
TSWV-PVR-S 3′ AGAUUCCAAUUCGAGUGAUUC 5′
(2777-2797)
B
Analysis of TSWV-induced symptoms in inoculated tissue
35S:GUS
TSWV-PVR + 35S:amiR-GUS
1
2
TSWV-PVR + 35S:amiR-TSWV-S
1
2
3
4
5
C
Analysis of TSWV-induced local lesions in inoculated tissue
Number of lesions
35S:GUS
35S:amiR-GUS
35S:amiR-TSWV-S
TSWV-PVR
D
Analysis of TSWV-induced symptoms in upper non-inoculated tissue
TSWV-PVR
35S:GUS
35S:amiR-GUS-1
35S:amiR-TSWV-S-1
E
Analysis of symptom appearance in upper non-inoculated tissue
%Plants with symptoms
DPI
35S:GUS
35S:amiR-GUS-1 + TSWV-PVR
35S:amiR-GUS-2 + TSWV-PVR
35S:amiR-TSWV-S-1 + TSWV-PVR
35S:amiR-TSWV-S-2 + TSWV-PVR
35S:amiR-TSWV-S-3 + TSWV-PVR
35S:amiR-TSWV-S-4 + TSWV-PVR
35S:amiR-TSWV-S-5 + TSWV-PVR
F
Analysis of TSWV accumulation in upper non-inoculated tissue
Absorbance
ab
0/6
6/6
35S:GUS
35S:amiR-GUS
35S:amiR-TSWV-S
TSWV-PVR

**FIGURE 6**

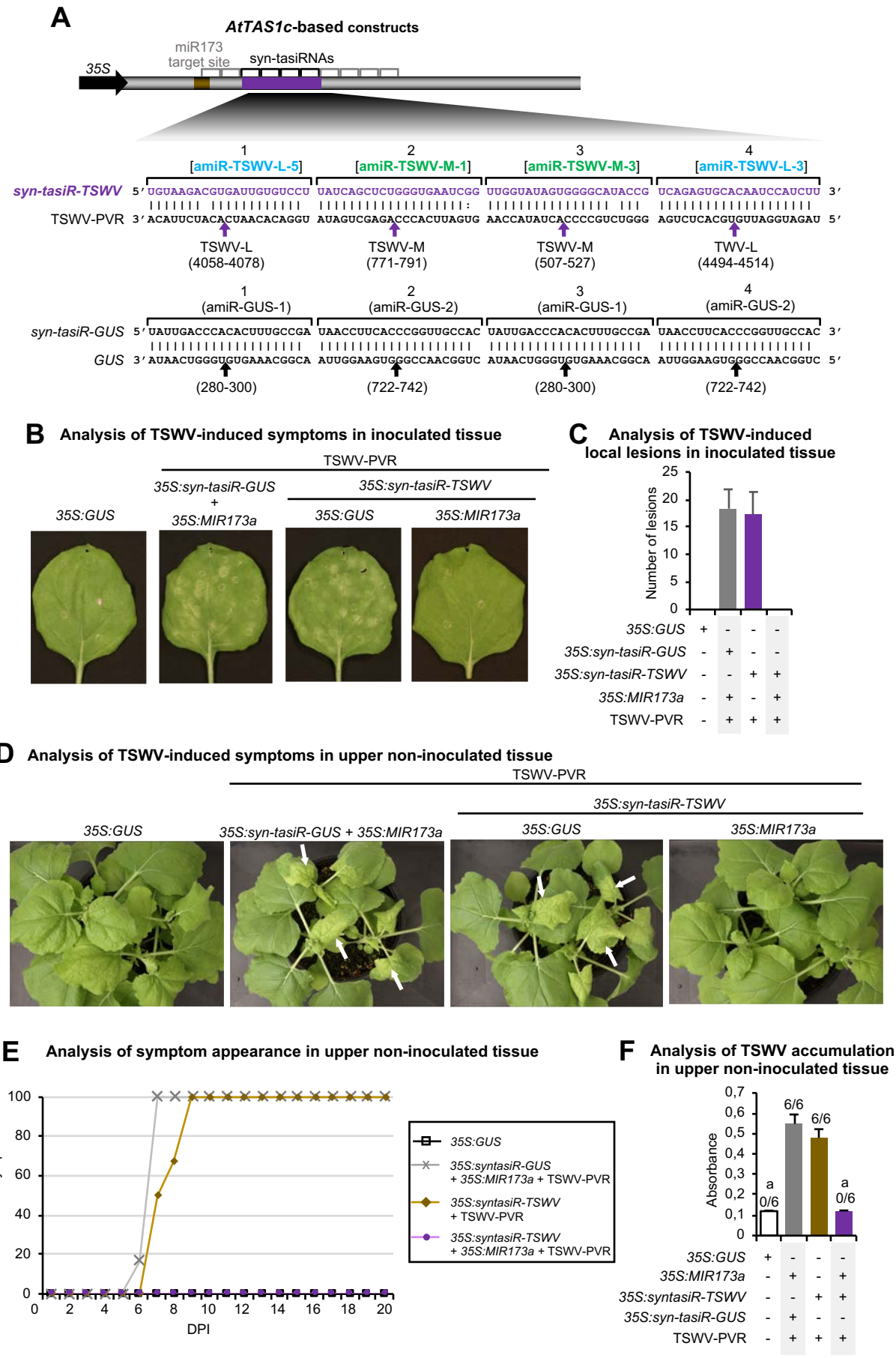
A
AtTAS1c-based constructs
miR173 target site
syn-tasiRNAs
35S
1 [amiR-TSWV-L-5]
2 [amiR-TSWV-M-1]
3 [amiR-TSWV-M-3]
4 [amiR-TSWV-L-3]
syn-tasiR-TSWV 5′ UGUAAGACGUGAUUGUGUCCU UAUCAGCUCUGGGUGAAUCGG UUGGUAUAGUGGGGCAUACCG UCAGAGUGCACAAUCCAUCUU 3′
TSWV-PVR 3′ ACAUUCUACACUAACACAGGU AUAGUCGAGACCCACUUAGUG AACCAUAUCACCCCGUCUGGG AGUCUCACGUGUUAGGUAGAU 5′
TSWV-L (4058-4078)
TSWV-M (771-791)
TSWV-M (507-527)
TWV-L (4494-4514)
1 (amiR-GUS-1)
2 (amiR-GUS-2)
3 (amiR-GUS-1)
4 (amiR-GUS-2)
syn-tasiR-GUS 5′ UAUUGACCCACACUUUGCCGA UAACCUUCACCCGGUUGCCAC UAUUGACCCACACUUUGCCGA UAACCUUCACCCGGUUGCCAC 3′
GUS 3′ AUAACUGGGUGUGAAACGGCA AUUGGAAGUGGGCCAACGGUC AUAACUGGGUGUGAAACGGCA AUUGGAAGUGGGCCAACGGUC 5′
(280-300)
(722-742)
(280-300)
(722-742)
B Analysis of TSWV-induced symptoms in inoculated tissue
TSWV-PVR
35S:syn-tasiR-GUS + 35S:MIR173a
35S:syn-tasiR-TSWV
35S:GUS
35S:GUS
35S:MIR173a
C Analysis of TSWV-induced local lesions in inoculated tissue
Number of lesions
25
20
15
10
5
0
35S:GUS + - - -
35S:syn-tasiR-GUS - + - -
35S:syn-tasiR-TSWV - - + +
35S:MIR173a - + - +
TSWV-PVR - + + +
D Analysis of TSWV-induced symptoms in upper non-inoculated tissue
TSWV-PVR
35S:syn-tasiR-TSWV
35S:GUS
35S:syn-tasiR-GUS + 35S:MIR173a
35S:GUS
35S:MIR173a
E Analysis of symptom appearance in upper non-inoculated tissue
%Plants with symptoms
100
80
60
40
20
0
0 2 4 6 8 10 12 14 16 18 20
DPI
35S:GUS
35S:syntasiR-GUS + 35S:MIR173a + TSWV-PVR
35S:syntasiR-TSWV + TSWV-PVR
35S:syntasiR-TSWV + 35S:MIR173a + TSWV-PVR
F Analysis of TSWV accumulation in upper non-inoculated tissue
Absorbance
0,7
0,6
0,5
0,4
0,3
0,2
0,1
0
a 0/6
6/6
6/6
a 0/6
35S:GUS + - - -
35S:MIR173a - + - +
35S:syntasiR-TSWV - - + +
35S:syn-tasiR-GUS - + - -
TSWV-PVR - + + +

FIGURE 7

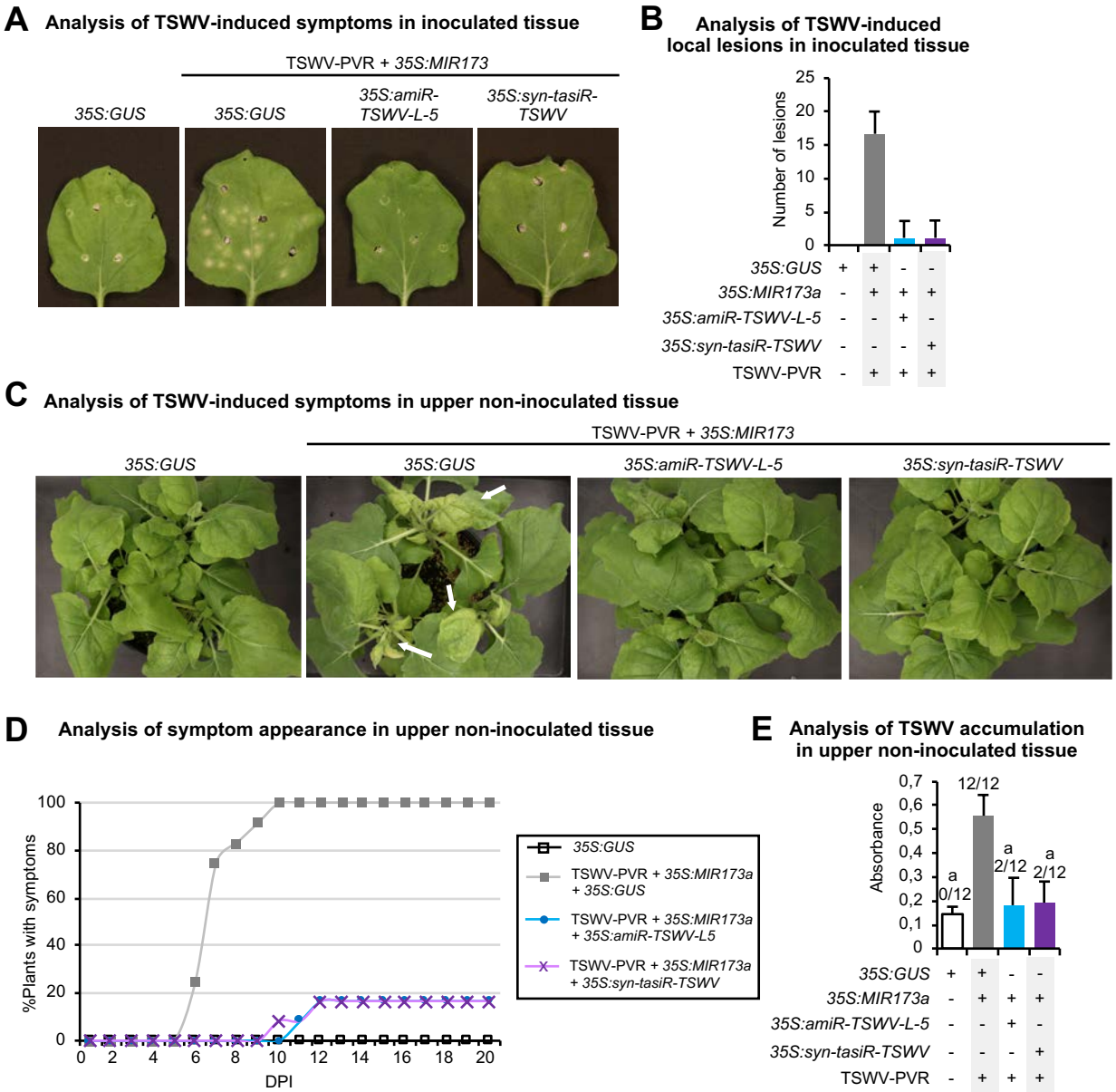
A
Analysis of TSWV-induced symptoms in inoculated tissue
TSWV-PVR + 35S:MIR173
35S:GUS
35S:GUS
35S:amiR-TSWV-L-5
35S:syn-tasiR-TSWV
B
Analysis of TSWV-induced local lesions in inoculated tissue
Number of lesions
25
20
15
10
5
0
35S:GUS + + - -
35S:MIR173a - + + +
35S:amiR-TSWV-L-5 - - + -
35S:syn-tasiR-TSWV - - - +
TSWV-PVR - + + +
C
Analysis of TSWV-induced symptoms in upper non-inoculated tissue
TSWV-PVR + 35S:MIR173
35S:GUS
35S:GUS
35S:amiR-TSWV-L-5
35S:syn-tasiR-TSWV
D
Analysis of symptom appearance in upper non-inoculated tissue
%Plants with symptoms
100
80
60
40
20
0
0 2 4 6 8 10 12 14 16 18 20
DPI
35S:GUS
TSWV-PVR + 35S:MIR173a + 35S:GUS
TSWV-PVR + 35S:MIR173a + 35S:amiR-TSWV-L5
TSWV-PVR + 35S:MIR173a + 35S:syn-tasiR-TSWV
E
Analysis of TSWV accumulation in upper non-inoculated tissue
Absorbance
0,7
0,6
0,5
0,4
0,3
0,2
0,1
0
a 0/12
12/12
a 2/12
a 2/12
35S:GUS + + - -
35S:MIR173a - + + +
35S:amiR-TSWV-L-5 - - + -
35S:syn-tasiR-TSWV - - - +
TSWV-PVR - + + +

**FIGURE 8**

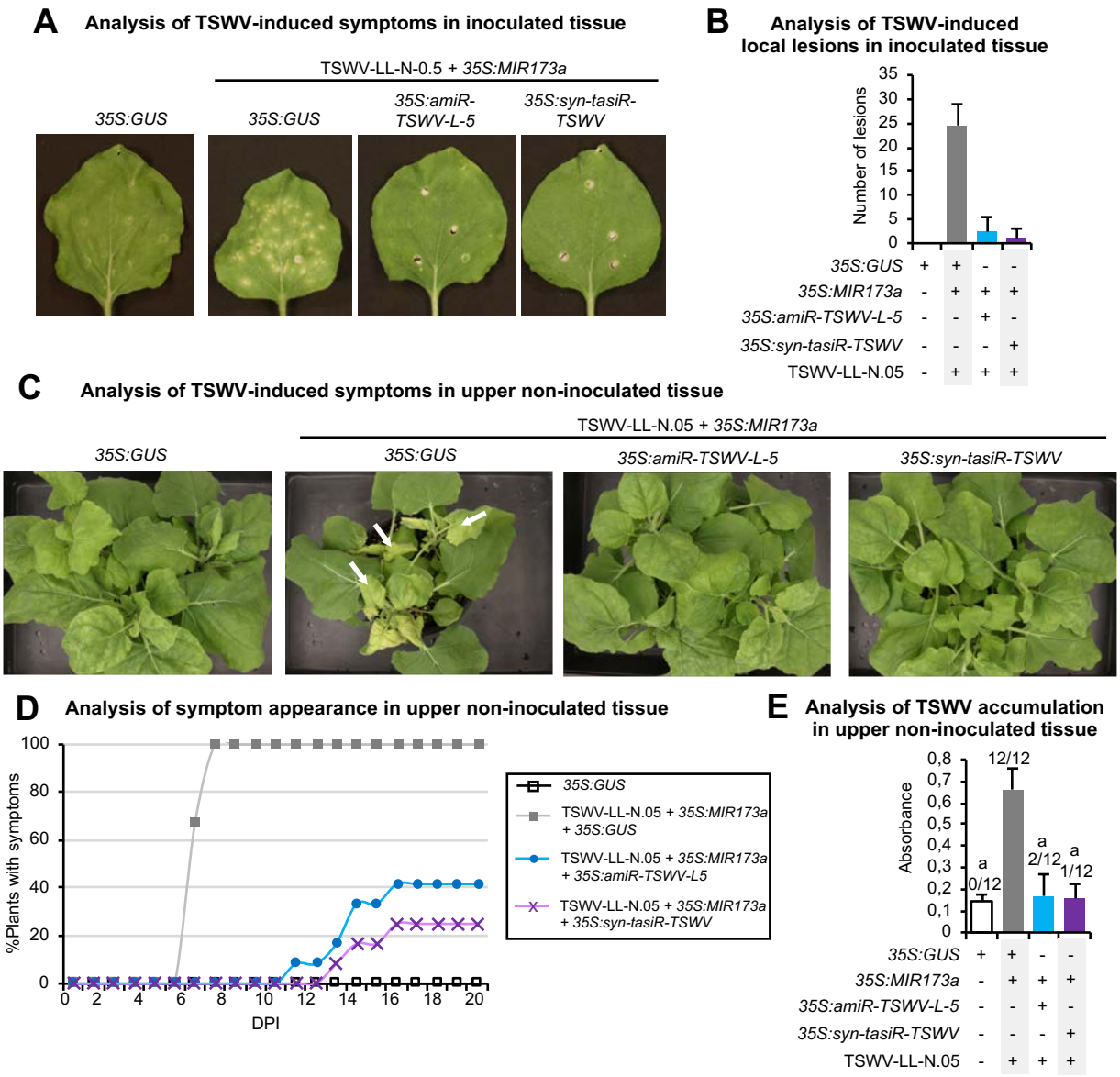
A
Analysis of TSWV-induced symptoms in inoculated tissue
TSWV-LL-N-0.5 + 35S:MIR173a
35S:GUS
35S:GUS
35S:amiR-TSWV-L-5
35S:syn-tasiR-TSWV
B
Analysis of TSWV-induced local lesions in inoculated tissue
Number of lesions
35S:GUS + + - -
35S:MIR173a - + + +
35S:amiR-TSWV-L-5 - - + -
35S:syn-tasiR-TSWV - - - +
TSWV-LL-N.05 - + + +
C
Analysis of TSWV-induced symptoms in upper non-inoculated tissue
TSWV-LL-N.05 + 35S:MIR173a
35S:GUS
35S:GUS
35S:amiR-TSWV-L-5
35S:syn-tasiR-TSWV
D
Analysis of symptom appearance in upper non-inoculated tissue
%Plants with symptoms
DPI
35S:GUS
TSWV-LL-N.05 + 35S:MIR173a + 35S:GUS
TSWV-LL-N.05 + 35S:MIR173a + 35S:amiR-TSWV-L5
TSWV-LL-N.05 + 35S:MIR173a + 35S:syn-tasiR-TSWV
E
Analysis of TSWV accumulation in upper non-inoculated tissue
Absorbance
a 0/12
12/12
a 2/12
a 1/12
35S:GUS + + - -
35S:MIR173a - + + +
35S:amiR-TSWV-L-5 - - + -
35S:syn-tasiR-TSWV - - - +
TSWV-LL-N.05 - + + +

FIGURE 9